POLITECNICO

MILANO 1863

The prognostic value of V-index in cardiovascular mortality in heart failure patients

TESI DI LAUREA MAGISTRALE IN
BIOMEDICAL ENGINEERING - INGEGNERIA BIOMEDICA

Author: **Luca Di Palma**

Student ID: 951672
Advisor: Prof. Valentina Corino
Co-advisors: Prof. Jose Felix Rodriguez Matas, Dr. Massimo Walter Rivolta
Academic Year: 2021-22

Abstract

The current study aims to investigate the prognostic value in heart failure (HF) patients of the $\mathcal{V}$-index, a new metric that has recently been proposed as an ECG marker quantifying spatial heterogeneity of ventricular repolarization. The population taken into consideration is composed of 380 sinus rhythm HF patients enrolled in the GISSI-HF Holter substudy [82% males, age 65 ± 10 years, non-sustained ventricular tachycardia (NSVT) incidence 44%, New York Heart Association (NYHA) functional class III–IV 20%, left ventricular ejection fraction (LVEF) 33 ± 8%]. After a follow-up of 43.1 ± 13.2 months, 55 patients died of cardiovascular causes, mainly associated with worsening HF or sudden cardiac death. In comparison to non-survivor, survivors had a reduced daily median $\mathcal{V}$-index value (median 29.65 ms [interquartile range (IQR) 22.51-37.42] vs. median 33.31 ms [IQR 25.68-46.02], Wilcoxon test, $p = 0.04$). In univariate Cox proportional-hazards analysis, a median $\mathcal{V}$-index value greater than 40 ms was associated with an increased risk of mortality [hazard ratio (HR): 2.23, 95% confidence interval (CI) 1.28-3.87, $p < 0.005$], also confirmed when adjuster for age [HR: 2.03, 95% CI 1.17-3.53, $p = 0.01$]. $\mathcal{V}$-index improved predictive performances, as quantified by the C-index, when added to clinical variables [age ≥ 70 years, serum creatinine ≥ 1.2mg/dL, LVEF, presence of NSVT]. The best model was obtained when combining the clinical model with a new signature [signature ≥ 15.25 ms, HR: 2.56, 95% CI 1.14-5.72, $p = 0.02$], derived from parameters obtained fitting the 24h $\mathcal{V}$-index data-points with a cosine function, obtaining a C-index of 0.78.

Keywords: heart failure, $\mathcal{V}$-index, cardiovascular mortality, Cox, survival analysis

Abstract in lingua italiana

Il presente studio ha lo scopo di indagare le capacità prognostiche nei pazienti con insufficienza cardiaca del $\mathcal{V}$-index, una nuova metrica che è stata recentemente proposta come marker ECG che quantifica l'eterogeneità spaziale della ripolarizzazione ventricolare. La popolazione presa in considerazione è composta da 380 pazienti con insufficienza cardiaca in ritmo sinusale arruolati nel sottostudio Holter del GISSI-HF [82% maschi, età 65 ± 10 anni, tachicardia ventricolare non sostenuta (NSVT) 44%, classe III-IV della New York Heart Association (NYHA) 20%, frazione di eiezione ventricolare sinistra (LVEF) 33 ± 8%]. Dopo un follow-up di 43.1 ± 13.2 mesi, 55 pazienti sono deceduti per cause cardiovascolari, principalmente associate al peggioramento dell'insufficienza cardiaca o alla morte cardiaca improvvisa. Rispetto ai partecipanti non sopravvissuti per cause cardiovascolari, i sopravvissuti presentano un minore valore mediano del $\mathcal{V}$-index giornaliero (mediana 29.65 ms [range interquartile (IQR) 22.51-37.42] vs. mediana 33.31 ms [IQR 25.68-46.02], Wilcoxon test, $p = 0.04$). Nell'analisi univariata di Cox, un valore mediano del $\mathcal{V}$-index superiore a 40 ms è associato a un aumento del rischio di mortalità [hazard ratio (HR): 2.23, intervallo di confidenza (IC) 95% 1.28-3.87, $p < 0.005$], così come quando combinato con l'età [HR: 2.03, IC 95% 1.17-3.53, $p = 0.01$]. Il $\mathcal{V}$-index ha migliorato le performance predittive, come quantificato dal C-index, quando è stato aggiunto alle variabili cliniche [età ≥ 70 anni, creatinina $\geq 1,2$ mg/dL, LVEF, presenza di NSVT]. Il modello migliore è stato ottenuto quando si è combinato il modello clinico con una nuova signature [signature ≥ 15.25 ms, HR: 2,56, IC 95% 1,14-5,72, $p = 0,02$], derivata da parametri ottenuti fittando i valori dei $\mathcal{V}$-index registrati nelle 24h con una funzione coseno, ottenendo un C-index di 0,78.

Parole chiave: insufficienza cardiaca, $\mathcal{V}$-index, mortalità cardiovascolare, Cox, analisi di sopravvivenza

Contents

Introduction

Motivation

Worldwide, an estimated 64.3 million people suffer from heart failure. One percent to two percent of the overall adult population in developed countries is estimated to have diagnosticated heart failure (HF). According to a meta-analysis of echocardiographic screening studies [1] in the general population, which included instances that had not yet been diagnosed, the prevalence of heart failure in industrialized nations is around 11.8% among those 65 and older. With this consideration, the estimated frequency in the general population would be 4.2%, which is about twice as high as other stated prevalence estimates based on registries with only confirmed cases. The difference between 4.2% and the 2% previously mentioned illustrates that even a prognostically severe syndrome such as heart failure may remain undetected in over half of the cases [2].

Goal

HF continues to be a leading cause of mortality globally, despite significant advancements in cardiovascular care throughout the late 20th century. Even while acute cardiovascular disease therapy has improved, efforts to stop the unavoidable decline are largely ineffective. Because there is currently no treatment for HF, the current clinical strategy focuses on managing the condition rather than finding a cure [3]. The main objective of the current study is to assess if the $\mathcal{V}$-index, a new metric that has recently been proposed as an ECG marker quantifying spatial heterogeneity of ventricular repolarization, can have a predictive value for cardiovascular mortality in HF patients, alone and when adjusted for clinical covariates such as age, left ventricular ejection fraction and serum creatinine level.

Outline

The contents of this thesis are organized as in the following.

In Chapter 1 HF is introduced, along with past studies which tried to identify what are the main predictors of mortality and morbidity in HF patients. Then, the $\mathcal{V}$-index and its applications in past researches are presented.

In Chapter 2, the dataset that has been used for the analysis is described. Then, the main algorithms that have been used in this thesis are presented. In section 2.2 the noise issue in ECG analysis and the CEEMD algorithm, which has been used to classify ECG segments as noisy or not, are described. Section 2.3 presents the mathematical steps to compute the $\mathcal{V}$-index. In section 2.4 the Cox model and the steps needed to find the best set of parameters β describing the hazard for the patients are reported, while in section 2.5 the cosinor analysis and its applications are delineated.

In chapter 3, the main results are collected. At first, a description of the distributions of the $\mathcal{V}$-index in the population is reported. Then, the results of the application of the Cox models are illustrated.

In Chapter 4 a final discussion on the $\mathcal{V}$-index predictive capabilities for cardiovascular mortality in HF patients is presented and compared with other indexes on the same population as well as with other studies analyzing HF patients.

1 | Preliminaries and Related Work

1.1. Heart Failure

HF is brought on by structural and functional myocardial abnormalities that limit ventricular filling or blood ejection. Possible causes of HF include dysfunction of the pericardium, myocardium, endocardium, heart valves, or great vessels alone or in combination. Increased hemodynamic overload, ischemia-related dysfunction, ventricular remodelling, excessive neuro-humoral stimulation, abnormal myocyte calcium cycling, excessive or insufficient extracellular matrix proliferation, accelerated apoptosis, and genetic mutations are a few of the main pathogenic mechanisms causing HF [3, 4].

Based on the location of the deficiency, HF can be categorized as predominantly left ventricular (LV), right ventricular, or biventricular. HF can be acute or chronic depending on the time of onset. Based on the heart's functional state, it is often divided clinically into two main types: HF with preserved ejection fraction (HFpEF) and HF with reduced ejection fraction (HFrEF). Ejection fraction (EF), which represents the amount (expressed as a percentage) of blood the left ventricle pumps out with each contraction, is frequently greater than 50% in patients with HFpEF, who are primarily female and older individuals. The LV cavity capacity is typically normal, but the LV wall is thickened and rigid, thus the ratio of LV mass/end-diastolic volume is high [5]. If the EF remains between 41% and 49%, HFpEF is further classified as borderline HF [3]. In contrast, the LV cavity is frequently dilated in individuals with HFrEF, and the ratio of LV mass to end-diastolic volume is either normal or decreased [4].

Four functional classifications of HF are identified by the New York Heart Association (NYHA) as follows:

- Class I: HF has no effects on physical activity restrictions, and typical physical activity has no symptoms.

- Class II: slight physical activity restrictions are brought on by HF; individuals are comfortable when at rest, but routine exercise brings on HF symptoms.

- Class III: HF significantly restricts physical activity; individuals are comfortable at rest, but symptoms of HF are brought on by less-than-normal exercise.

- Class IV: patients with HF have symptoms while at rest or are unable to engage in any physical activity without experiencing HF symptoms.

Exercise intolerance, defined as a decrease in peak $VO2/VO2_{max}$ capacity ($VO2_{max}$ is the greatest amount of oxygen a person can take in when exercising), has been identified as the main predictor of mortality and morbidity in HF patients. Additional factors that have been identified as independent predictors of mortality include older age, higher blood urea nitrogen, creatinine and heart rate, lower systolic pressure and serum sodium, the presence of dyspnea at rest, absence of long-term beta-blocker (BBL) treatment, male gender and lower body mass index and haemoglobin levels.

Other predictors that have been reported in [4] and demonstrated in [6–8] to be associated with bad outcomes for HF patients are:

- High NYHA functional class

- Reduced left ventricular ejection fraction (LVEF)

- Third heart sound

- Increased pulmonary artery capillary wedge pressure

- Reduced cardiac index

- Diabetes mellitus

- Reduced sodium concentration

- Raised plasma catecholamine and natriuretic peptide concentrations

In particular, critical thresholds that have been shown to predict increased mortality in [9–12] are reported:

- Serum urea >15 mmol/L

- Systolic blood pressure <115 mmHg

- Serum creatinine >2.72 mg/dL (or 240 μmol/L)

- N-terminal pro-brain natriuretic peptide (NT-pro-BNP) >986 pg/mL

- LVEF <45%

Several studies have been conducted in order to find relevant variables to identify HF patients with a greater risk of death. Ahmad et al. [13] investigated a population of 299 heart failure patients (105 women and 194 men), aged 40 years or above, having left ventricular systolic dysfunction, belonging to NYHA classes III and IV. After a follow-up of 4–285 days, with an average of 130 days, 96 (32%) patients died due to cardiovascular heart disease (CHD). Age, ejection fraction, serum creatinine, serum sodium, anaemia, platelets, creatinine phosphokinase (CPK), blood pressure, gender, diabetes, and smoking status were all taken into account when modelling mortality using Cox regression. Analyzing the Cox regression coefficient, authors found out that chances of death due to CHD increase with growing age, with an increment of 4% risk of dying every additional year of age. Another important aspect was EF; having an EF $\leq$ 30 % corresponds to hazard rates that were 67% and 59% greater than those with 30%<EF$\leq$45% and EF $\geq$45%, respectively. Serum creatinine and serum sodium assume relevant significance, resulting in an increase of the risk of mortality by more than twice for every unit rise in serum creatinine, while one unit (meq/L) increase in serum sodium decreases the hazard by 6%. While anaemia was a significant variable (anaemic patients had 76% higher mortality rates compared to non-anaemic patients), gender, smoking, diabetes, CPK, and platelets were not significant.

Similar results except for the significance of gender and diabetes can be found in [14], where Barlera et al. examined 6975 patients with chronic heart failure enrolled in the Gruppo Italiano per lo Studio della Sopravvivenza nell'Infarto Miocardico-Heart Failure (GISSI-HF) trial. During a median follow-up of 3.9 years, 1969 patients died. Age was the most effective predictor of mortality when taking into account all of the factors statistically significant in the univariate analysis ($p < 0.05$), with a linear rise in risk of 4% for each year. Other important predictors that authors found were estimated glomerular filtration rate (eGFR), showing an increase of 1.6% in hazard for every unit decrease in eFGR (when eGFR$\leq$60), LVEF (every unit decrease in EF<40% brought to a 2.5% increase in hazard), the presence of chronic obstructive pulmonary disease and a severe NYHA class (III+IV) strongly increased the hazard, by 33% and 28%, respectively. Diabetes mellitus, male sex, aortic stenosis, ischemic aetiology, peripheral edema, and >1 previous hospitalization for HF were independent, highly significant predictors of death.

La Rovere et al. [15] analyzed 388 patients (of the 6975 patients of the GISSI-HF trial) in sinus rhythm who carried out a 24 h digital Holter recording at the time of enrolment. The authors analyzed differences between alive and dead (for cardiovascular reasons) patients, finding out that patients who passed away were older, had a more advanced NYHA class, lower left ventricular function, a greater frequency of NSVT, worsened renal function, and

had less BBL treatment. Considering a multivariate Cox regression model, they identified the following clinical variables as those that carried the highest joint predictive value in the examined population: age $\geq$70 years [hazard ratio (HR) 3.09, 95% confidence interval (CI) 1.80–5.30, $p < 0.001$], LVEF (HR 0.96, 95% CI 0.93–0.99, $p = 0.025$), presence of NSVT (HR 2.17, 95% CI 1.24–3.81, $p = 0.007$), and serum creatinine level (HR 1.72, 95% CI 1.37–2.15, $p < 0.0001$), obtaining a C-index of 0.753. Then, they investigated the effect of adding to the clinical model autonomic markers of the ECG. In particular, they computed the standard deviation of all normal-to-normal RR intervals (SDNN), the power in the very low-frequency bands (VLFP, 0.01–0.04 Hz) and in low-frequency bands (LFP, 0.04–0.15 Hz) that were then both log-transformed, the short-term fractal scaling exponent measured by the detrended fluctuation analysis method (DFA), the turbulence onset (TO), the turbulence slope (TS) and the deceleration capacity (DC). Combining independently these markers with the clinical model, they obtained a C-index of 0.763, 0.790, 0.788, 0.763 and 0.755, for SDNN, Ln VLFP, Ln LFP, DFA and TS, respectively.

1.2. $\mathcal{V}$-index

In the last years, a novel index has been proposed by Sassi and Mainardi [16]. The $\mathcal{V}$-index is an ECG-based estimator of the standard deviation (s_θ) of ventricular myocytes' repolarization times (ρ_m) across the entire myocardium, obtained from multi-leads surface ECG. The spatial heterogeneity of ventricular repolarization (SHVR) gives rise to the T-wave in the human heart. However, amplification of this dispersion is a perpetrator of ventricular arrhythmias. As a result, it would be clinically useful to determine repolarization heterogeneity from the ECG to predict life-threatening ventricular arrhythmias and pharmacological adverse effects on the cardiovascular system.

Several research studies have been conducted on the $\mathcal{V}$-index. Abächerli et al. [17] have assessed the abilities of the $\mathcal{V}$-index by performing a large observational cohort study to examine the diagnostic and prognostic values of the $\mathcal{V}$-index in 767 unselected patients presenting to the emergency department with symptoms suggestive of non-ST-elevation myocardial infarction (NSTEMI), and a narrow QRS complex. They found out that, when compared to patients with other types of chest pain, individuals with acute myocardial infarction (AMI) had higher $\mathcal{V}$-index values (median 23 ms vs. 18 ms, $p = 0.001$). In addition to the traditional ECG criteria, the introduction of the $\mathcal{V}$-index increased the sensitivity of the ECG for AMI from 41% to 86% and the diagnostic accuracy for the diagnosis of NSTEMI as measured by the area under the ROC curve from 0.66 to 0.73 ($p = 0.001$). Also, while evaluating the prognostic value of the $\mathcal{V}$-index for the prediction

of mortality during follow-up, they found that median $\mathcal{V}$-index levels in deceased patients were significantly higher as compared to those in survivors (28ms (IQR 22–38) vs. 18 ms (IQR 15-24), $p < 0.001$). Assessing the prognostic value for the prediction of death by ROC curve analysis showed an AUC for the $\mathcal{V}$-index of 0.83 (95% CI 0.73–0.92) resulting in significantly better with respect to the score of conventional ECG criteria (AUC 0.63, 95% CI 0.47–0.78, $p = 0.002$ for comparison).

In [18], $\mathcal{V}$-index performance to assess changes of the SHVR was evaluated after moxifloxacin and sotalol administration and compared with the corrected QT interval (QT_c). These two drugs are known to change the QT interval duration in distinct ways, varying from subtle (moxifloxacin) to clearly perceptible (sotalol). Comparing the effects of these drugs on two populations, both $\mathcal{V}$-index and QT_c increased along with the drugs' serum concentration. With sotalol the two metrics displayed evident changes ($\mathcal{V}$-index: 27.79 ms $\pm$ 4.89 ms versus 60.13 ms $\pm$ 18.52 ms; QT corrected: 387.07 ms $\pm$ 19.84 ms versus 437.76 $\pm$ 32.05 ms; $p < 0.05$) while regarding moxifloxacin, values slightly changed for $\mathcal{V}$-index (30.70 ms $\pm$ 8.32 ms versus 40.48 ms $\pm$ 7.61 ms; $p < 0.05$), and for QT_c (404.29 ms $\pm$ 29.05 ms versus 426.77 $\pm$ 36.67 ms; $p < 0.05$). With both drugs, the maximal percentage variation after administration was higher for $\mathcal{V}$-index than QT_c (moxifloxacin: 34.56% $\pm$ 24.60% versus 5.56% $\pm$ 2.98%; sotalol: 114.77% $\pm$ 33.15% versus 12.13% $\pm$ 2.85% ; $p < 0.05$). In conclusion, the authors claimed that the standard deviation of the ventricular repolarization times, as quantified by the $\mathcal{V}$-index, might be an effective measure of spatial heterogeneity and also showed evidence in the applicability for assessing drug-induced pro-arrhythmic effects.

Corino et al. [19] aimed to assess the effect of four drugs blocking the human ether-à-go-go-related gene (hERG) potassium channel, alone or in combination with other ionic channel blocks, on SHVR, as estimated by the $\mathcal{V}$-index on short triplicate 10s ECG. Twenty-two healthy subjects received a pure hERG potassium channel blocker (dofetilide) and 3 other drugs with additional varying degrees of sodium and calcium (L-type) channel block (quinidine, ranolazine, and verapamil), as well as placebo. Indeed, it is generally recognized that several drugs, whether anti-arrhythmic or not, can have harmful cardiovascular effects and have been linked to drug-induced arrhythmias. Some, such as class III antiarrhythmic drugs, may extend repolarization and cardiac refractoriness while also increasing the spatial heterogeneity of ventricular repolarization. Determining if they block important ion channels can be crucial to identify pro-arrhythmic drugs. Among the many, a relevant pro-arrhythmic block is the one that occurs to the hERG potassium channel (outward current). Drugs that block the hERG potassium channel may also simultaneously block calcium and/or sodium channels (inward currents), which might have

a "compensatory" impact, therefore not all of them are necessarily linked with a significant pro-arrhythmic risk. Therefore, the interest of the authors has been focused on those drugs having a compensatory effect, seeming to be safer to use. Results of the study showed that, after administering either dofetilide or quinidine, the $\mathcal{V}$-index experiences significant growth. On the other hand, neither the administration of verapamil nor ranolazine was related to a substantial change in the $\mathcal{V}$-index. Thus, the $\mathcal{V}$-index was found to increase only with drugs associated with torsade risk, encouraging its use in detecting the risk of torsade of antiarrhythmic drugs.

Rivolta et al. [20] investigated whether or not cardiac SHVR in people with chronic Chagas disease could be linked to a higher chance of dying. Utilizing the $\mathcal{V}$-index, repolarization heterogeneity was evaluated. Between 1998 and 1999, 113 patients (aged 21 to 67) who had known serological statuses indicating positive responses to Trypanosoma cruzi were recruited. Over the course of a 10-year follow-up period, 14 participants passed away. In comparison to non-survivor participants, survivors had a substantially reduced $\mathcal{V}$-index (31.2 $\pm$ 13.3 vs. 41.2 $\pm$ 18.6 ms; single-tail t-test, $p = 0.009$; single-tail Wilcoxon rank sum test, $p = 0.029$). In a univariate Cox proportional-hazards analysis, a $\mathcal{V}$-index greater than 36.3 ms was associated with a substantially increased risk of mortality (HR $= 5.34$, $p = 0.0046$). Additionally, even with shrinkage, a statistical technique that guards against over-fitting because of the small sample size, $\mathcal{V}$-index > 36.3 ms maintained its prognostic value in a multivariate Cox proportional-hazards analysis after adjustment for the other three clinical variables (left ventricular ejection factor<0.50, QRS duration > 133 ms, ventricular tachycardia during stress testing or 24 hours Holter), as well as for T-wave amplitude. The results of the study demonstrated a significant correlation between the risk of mortality in univariate survival analysis and a higher dispersion of repolarization times in Chagas disease patients, as assessed by the $\mathcal{V}$-index. The $\mathcal{V}$-index collects prognostic data that are not readily accessible through the examination of other recognized risk variables.

Rivolta et al. in [21] aimed to assess SHVR as a predictor of cardiovascular (CV) death and/or other CV events in patients with atrial fibrillation (AF). 1711 patients were included in the study, from the multicenter prospective Swiss-AF Cohort Study who were in sinus rhythm (995) or AF (716). At baseline, 5-min long resting ECG recordings were acquired. Four parameters measuring ventricular repolarization were computed (QTc, Tpeak-Tend, J-Tpeak and $\mathcal{V}$-index). The $\mathcal{V}$-index was shown to be reproducible during AF (no differences when computed over the whole recording, on the first 2.5-min and on the last 2.5-min segments). 90 patients passed away from CV causes throughout the course of a mean follow-up period of 2.6 $\pm$ 1.0 years. The $\mathcal{V}$-index and QT_c were linked to

an elevated risk of CV mortality in multivariate analysis adjusted for clinical risk variables and medications (QT_c: [HR: 2.78, 95% CI 1.79-4.32, $p < 0.001$;] $\mathcal{V}$-index: [HR 1.73, 95% CI 1.12-2.69, $p = 0.014$]). The study demonstrated that in a cohort of patients with AF, QT_c and $\mathcal{V}$-index, evaluated in a single 5-min ECG recording, were independent predictors of CV mortality and HF hospitalization and they may be useful for additional risk classification to help with patient treatment.

2 | Material and Methods

2.1. Population

The dataset that has been used for the analysis is part of the GISSI (Gruppo Italiano per lo Studio della Sopravvivenza nell'Infarto miocardico) dataset.

The goal of the GISSI-HF [22] study, which was a randomized placebo-controlled trial, was to determine the effects of n-3 polyunsaturated fatty acids and rosuvastatin on mortality and morbidity in patients with clinical indications of stable chronic HF, regardless of the underlying causes, levels of LVEF, or age. All patients provided informed permission, and the study was authorized by the institutional review boards at each participating facility. Between August 2002 and February 2005, 325 cardiology and 31 internal medicine facilities in Italy enrolled a total of 6,975 ambulatory patients with chronic HF. At study enrollment, at 1-, 3-, 6-, and 12-month follow-up visits, and then every 6 months until the end of the trial, comprehensive clinical data including patient characteristics, medical history, physical examination, 12-lead electrocardiogram, laboratory results, and medication use were collected. Within three months of enrolment, patients were required to have their LVEF evaluated. The patient had to have had at least one hospital admission for HF in the year prior if LVEF was >40%. Congestive heart failure medications that were optimized for each patient were also strongly advised [23].

The study included a Holter sub-study to assess Holter-derived autonomic variables. For the purpose of the sub-study, 390 sinus rhythm patients out of the 6975 research participants completed a 24-hour digital Holter recording at the time of enrollment in 41 enrolling centers. Men and women who were 18 years of age or older, had clinical evidence of HF from any cause and had any LVEF, were eligible patients.

A 12-lead digital Holter monitoring system with high resolution (1000 Hz) was used for the recordings (model H12 +, Mortara Instruments, Milwaukee, WI, USA). The Holter analysis program initially classified each beat as normal or aberrant before being meticulously confirmed by a professional analyst. Annotated RR time series were transmitted to a computer using specialized software (SuperECG, Mortara Instruments). The research

only accepted recordings that could be analyzed for at least 12 hours [15].

In the present study, 380 patients have been considered as participants in the first visit. 8 of the 388 patients (two of the 390 patients were excluded having less than 12h analysable ECG recordings) enrolled in the previous study [15] were excluded due to the fact that ECG recordings were not available. Table 2.1 summarizes the characteristics of the entire population that has been involved in the current study. After a follow-up of 43.1 ± 13.2 months, 55 patients died of CV causes, mainly associated with worsening HF or sudden cardiac death.

Variable	Entire population
Age (years), mean ± std	64.76 ± 10.39
Gender (M)	313 (82%)
LVEF (%), mean ± std	32.36 ± 8.38
NSVT	166 (44%)
Creatinine (mg/dL), mean ± std	1.17 ± 0.48
Sodium (mEq/L), mean ± std	140.1 ± 3.9
Potassium (mEq/L), mean ± std	4.47 ± 0.49
Bilirubin (mg/dL), mean ± std	0.76 ± 0.36
NYHA class III-IV	77 (20%)
ACE	357 (94%)
Beta-blockers	263 (69%)
Diuretics	320 (84%)
Digitalis	86 (23%)
Nitrates	125 (33%)
Amiodarone	60 (16%)
Ischaemic cardiomyopathy	192 (51%)

Table 2.1: Demographic and clinical characteristics in the entire population. M: male; ACE: angiotensin-converting enzyme.

2.2. Noise Detection

2.2.1. Noise issue in ECG analysis

The creation of an automatic and reliable ECG analysis system for screening or monitoring heart diseases can greatly benefit from the classification and automatic detection of noise. The analysis of the ECG can be severely impacted by noise, in some situations making it impossible to make a clear differentiation of the major ECG complexes (P-wave, QRS, T-wave). This could lead to erroneous beat identification, poor measurements of crucial ECG parameters as the RR interval, and ultimately prevent accurate analysis. Noise could potentially cause normal heartbeats to be mistaken for arrhythmias, which would intensify the alarm fatigue issue [24].

In particular, ECG signals are typically corrupted by different types of noise or artefacts:

- Powerline interference (PLI)

- Baseline wander (BW) and motion artefacts

- Muscle artefacts (MA)

The PLI is a narrowband noise with an amplitude up to 50% of the peak-to-peak ECG amplitude, centered at 50/60 Hz, and a bandwidth less than 1 Hz [25]. The detached electrode, which produces an extremely potent and distressing signal, is the most frequent source of this interference. Contacts on the patient's cable and unclean electrodes can also cause PLI [26]. The low-amplitude local waves of the ECG signal can have their shape, duration, and morphological characteristics distorted by severely structured noises. Particularly, P-wave distortions can cause atrial arrhythmias like atrial enlargement and fibrillation to be misdiagnosed [27].

Respiration, changes in electrode impedance, and body movement can all contribute to baseline drift. BW can hide significant ECG information, and if it is not correctly eliminated, the ECG's vital diagnostic data will be lost or damaged [28]. The BW frequency spectrum spans from 0.05 to 1 Hz. At frequencies between 0.15 and 0.3 Hz, the respiration baseline wander's amplitude varies by about 15% of the peak-to-peak ECG's amplitude. The motion artefact, which is a rapid drift brought on by variations in the electrode-skin impedance due to the motion, has an amplitude 500 percent larger than the peak-to-peak ECG and lasts between 300 and 500 milliseconds. The ST segment and other low-frequency (LF) components of the ECG signal can be distorted by severe BW or motion artefacts.

The electrical activity of muscles during periods of contraction or as a result of a sudden body movement is what causes muscle artefacts (or EMG). An EMG noise typically has a bandwidth between 20 and 1000 Hz and an amplitude that is about 10% of the ECG amplitude. According to some studies, the frequency range has an average amplitude of 10% level and ranges from dc to 10,000 Hz [25]. Since the frequency of EMG noise and the frequency of the ECG signals, which is in the range of 0.01-100 Hz, significantly overlap, previous studies have shown that the MA can significantly alter the shapes of local waves of the ECG signal [29].

To deal with all these problems, several approaches have been used to address the issue of the high false alarm rate caused by noises and artefacts:

- ECG denoising-based strategy to suppress the noises and artefacts in the ECG recordings.

- Signal quality index (SQI)-based strategy to judge the clinical acceptability of the recorded ECG signals.

ECG denoising-based strategy consists of several methods, including moving average and median filters, frequency-selective filters, adaptive filters, Wiener filters, polynomial filters, singular value decomposition, discrete cosine transform, discrete wavelet transform, empirical mode decomposition (EMD), nonlinear Bayesian filter, mathematical morphological operators, independent component analysis, nonlocal means method, variational mode decomposition and EMD-wavelet method for removal of single and combined ECG noise sources [27].

In addition to the noise reduction approach, the signal quality assessment (SQA) strategy has been used to classify the recorded ECG signals as acceptable or undesirable. According to Satija et al. [27], the SQA methods can be grouped into five categories:

- Fiducial points and heuristic rules-based (FP-HR) SQA methods;

- Fiducial points and machine learning-based (FP-ML) SQA methods;

- Nonfiducial points and heuristic rules-based (NP-HR) SQA methods;

- Nonfiducial points and machine learning-based (NP-ML) SQA methods;

- Filtering-based SQA methods

A set of morphological and interval features, such as the duration and amplitude of P-waves, QRS complexes, T-waves, PR and ST segment intervals, and QT and RR intervals are extracted from single or multi-lead ECG signals and combined with heuristic rules

with predefined decision thresholds in FP-HR-based SQA methods.

FP-ML SQA methods calculate sets of interval and morphological characteristics from the ECG signals initially and then train a classifier to recognize various noise patterns and ECG signal types.

From the ECG signals, NP-HR SQA algorithms frequently extract sets of the time-domain, frequency-domain, time-frequency domain, statistical, and information-theoretic features, while in NP-ML SQA methods different SQIs are computed and then feed to a classifier.

Filtering-based SQA methods include filtering techniques which were applied for the assessment of noise corruption levels, such as SQI-Modified Kalman Filter (KF) [30] and multichannel adaptive filtering [31].

2.2.2. Modified CEEMD Algorithm

In this study, the algorithm used in order to detect noise and get the SQA index of the ECG is the one proposed by Satija et al. in [32]. Even if the proposed algorithm allows not only the identification but also the classification of different types of ECG noises, for the purpose of this study the algorithm was only used to detect the noise presence.

The modified complete ensemble empirical mode decomposition (CEEMD) method is used to first break down ECG signals to distinguish the ECG components from noise and artefacts. Then, using the recovered high-frequency and LF signals, the short-term temporal properties of the autocorrelation function are calculated, including its maximum absolute amplitude (MAA) and the number of zero-crossings (NZC). In the end, a decision rule-based approach is described for identifying the existence of noise and classifying it into six signal groups: noise-free ECG, ECG+BW, ECG+MA, and ECG+PLI.

The EMD is frequently used to break down complicated multi-component signals into a number of fast and slow oscillations known as intrinsic mode functions (IMFs). The CEEMD technique has been proposed to address the limitations of the basic EMD and ensemble EMD (EEMD), as the mode mixing issue, where different oscillations exist in the same IMF or similar oscillations exist in different IMFs producing a variable number of IMFs, and reconstructed signals contain residual noise after decomposition when the signal to noise ratio is low. The CEEMD algorithm was proposed by Torres et al. [33], in which they add different realizations of gaussian noise to the residual signal after extracting subsequent IMFs. A signal is decomposed using the CEEMD algorithm into a finite set of IMFs (or oscillation modes) and a residue. Until the resulting residue is no longer decomposable, or until a predefined threshold is achieved, the decomposition

procedure is continued. Lower-order IMFs generally capture rapid oscillation patterns of high-frequency noises produced by MA, PLI, and recording devices, whereas higher-order IMFs frequently capture slow oscillation modes of BW.

The modified CEEMD algorithm, proposed to reduce the computational load of the conventional CEEMD algorithm, stops when the magnitude of the current residue is less than the predefined threshold or when the number of zero-crossings of the current residue is less than the predefined NZC value.

The steps followed by the algorithm for a given ECG signal $x[n]$ are:

1. Obtain different realizations of signal plus white Gaussian noise $w^k[n]$ of standard deviation ϵ, i.e., $x^k[n] = x[n] + w^k[n]$, with $k = 1....K$, where K denotes the total number of realizations.

2. Decompose the signal plus noise realizations $x[n] + \epsilon_0 w^k[n]$ using EMD to get their first IMFs and then compute the first IMF as

$$\overline{IMF_1}[n] = \frac{1}{K} \sum_{k=1}^{K} IMF_1^k[n]$$

3. Compute first residue as $r_1[n] = x[n] - \overline{\text{IMF}_1}$

4. Decompose realizations $r_1[n] = x[n] + \epsilon_1 w^k[n]$ to get their first EMD mode and obtain the second mode:

$$\overline{IMF_2}[n] = \frac{1}{K} \sum_{k=1}^{K} E_1(r_1[n] + \epsilon_1 w^k[n])$$

   where E_1 denotes first mode from EMD decomposition.

5. For finding the i_{th} mode, decompose realizations of the i_{th} residue, $r_1[n] = x[n] + \epsilon_1 w^k[n]$ to get their first EMD mode and obtain the $(i+1)_{th}$ mode as

$$\overline{IMF_{(i+1)}}[n] = \frac{1}{K} \sum_{k=1}^{K} E_1(r_i[n] + \epsilon_i w^k[n])$$

$$i = 1, 2, ...I$$

   where I denotes the total number of modes and $r_i[n] = r_{(i-1)}[n] - \overline{IMF_i[n]}$

6. Compute the NZC and the MAA for the $IMF_i[n]$.

7. Continue step 5 for the next mode until the obtained residue does not satisfy the proposed stopping criteria: $if(NZC > 10||MAA > 0.1)$ is true.

An example of the IMFs obtained by the CEEMD decomposition is illustrated in Figure 2.1. Higher-order IMFs catch extremely LF components of the local waves for the noise-free ECG signals, whereas lower-order IMFs capture rapidly changing components of QRS complexes. For the noisy ECG signals instead, lower-order IMFs capture the high-frequency components of the MA, PLI noises, and QRS complexes. In both situations, the BW components are included in the final residue.

In order to solve the noise classification problem, they built three signals, as illustrated in Figure 2.2:

- $h[n]$: it is the high-frequency signal, obtained by summing the first tree IMfs.

- $b[n]$: it is the LF signal, so the final residue, representing the baseline wander.

- $c[n]$: it is the ECG signal, obtained by adding remaining IMFs, which include the major components of P-wave, QRS-complex and T-wave.

Peak-to-peak amplitudes of the extracted $h[n]$ and $b[n]$ can be used to investigate the presence and severity of the noises and artefacts. For detecting the presence of BW noises, the MAA feature is extracted from the final residual signal $b[n]$. Based on the amplitude ranges of the local waves such as P-wave, Q-wave, QRS-complex, and T-wave, the MAA threshold of $0.1mV$ is chosen in [34]. The MAA of the high-frequency signal $h[n]$ is instead used to investigate the severity of the high-frequency noises. The MAA threshold of $0.05mV$ is chosen for detecting the presence of MA and PLI noises. Noise-specific features such as short-term zero-crossing and autocorrelation features are used for the detection and classification of high-frequency noises. The extracted high-frequency signal $h[n]$ is first divided into overlapping frames with a frameshift of one sample. The overlapping process is implemented as $h_k[n] = h[k + n], n = 0, 1, 2, ...N - 1$ where $k = 0, 1...L - M - 1$. $h_k[n]$ is the k_{th} frame and M denotes the frame size. Then, the NZC is computed for frames of $h[n]$. The NZC feature envelope is computed as

$$f(n) = \begin{cases} Compute\ NZC, & \text{if } max(|h_k[n]|) > 0.05 \\ 0, & otherwise \end{cases}$$
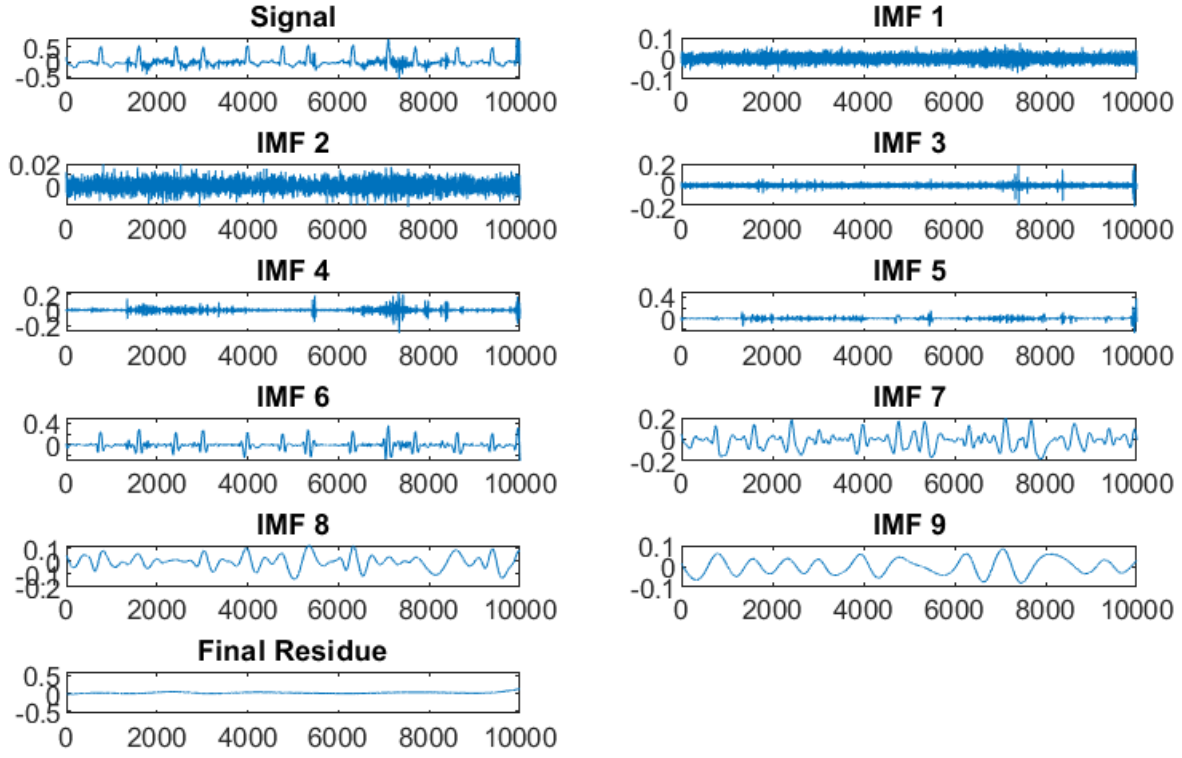
Figure 2.1: An example of the decomposition process of the CEEMD algorithm.

For detecting the presence of high-frequency noises, the gate signal is computed as

$$g(n) = \begin{cases} 1, & \text{if } NZC[n] > 1 \\ 0, & otherwise \end{cases}$$

Temporal characteristics like MAA and NZC are used to identify baseline drift. The BW noise detection rule is defined as

$$BW = \begin{cases} Yes, & \text{if } max(|b[n]|) > 0.1 \ \& \ (NZC < 10) \\ No, & otherwise \end{cases}$$

The severity of the high-frequency noises is defined based on the MAA of $h[n]$. If the MAA of $h[n]$ is greater than a predefined threshold of $0.05mV$, $h[n]$ is further processed to obtain $g[n]$ from the NZC envelope. Otherwise, the ECG signal is detected as a high-frequency noise-free ECG signal. The local pulse widths corresponding to the QRS complex components generally range between 50 and 300 ms, according to gate signals derived on noise-free ECG. ECG signals corrupted with MA and PLI noises appear in
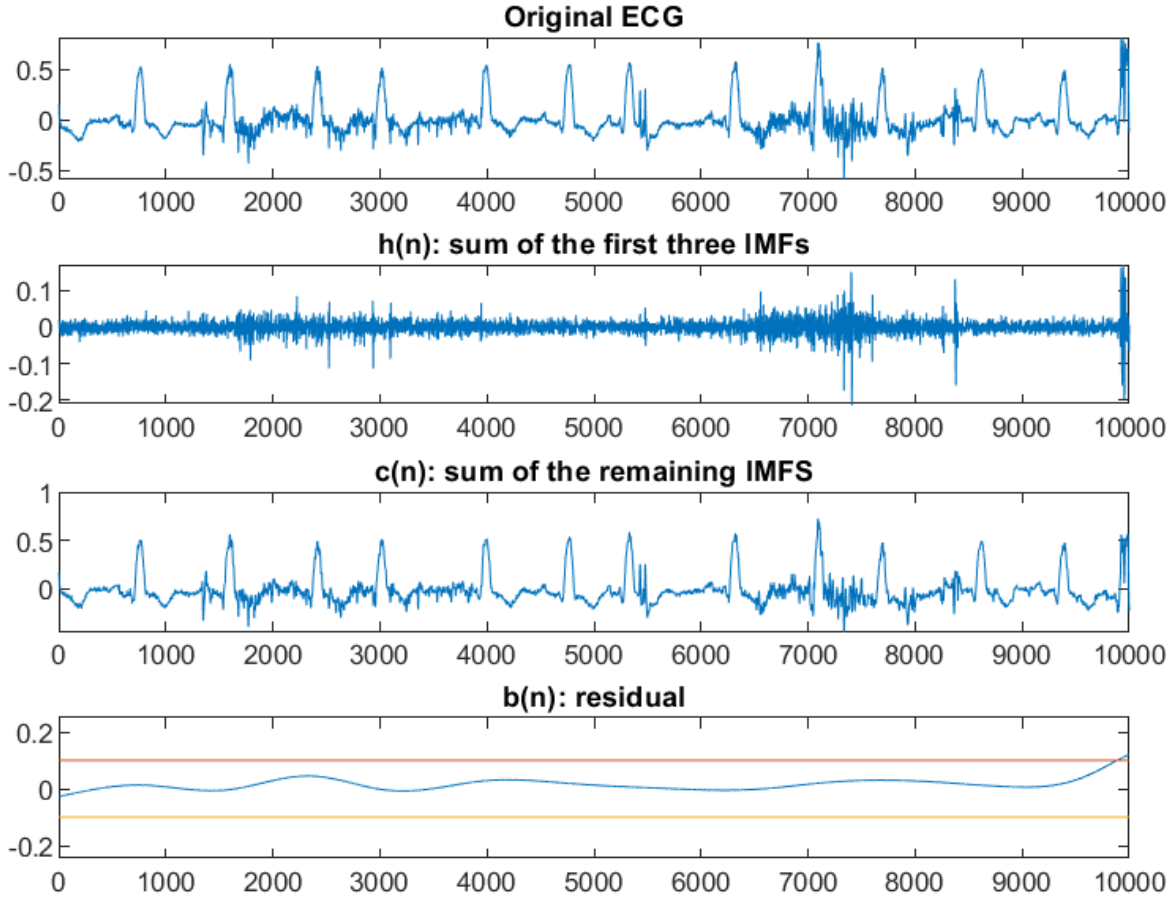
Figure 2.2: An example of the ECG split in the 3 signals obtained from the IMFs.

the gate signals with local pulses of extremely short duration and longer duration. To distinguish QRS complex pulses from noise frames in $h[n]$, the pulse width thresholding rule is used with the QRS width duration (50-200 ms) and refractory period (200-300 ms) parameters. To detect the presence of high-frequency noise, as represented in Figure 2.3, the duration of each of the local pulses is compared with the predefined lower and upper duration thresholds. The high-frequency noise detection rule is defined as

$$high\text{-}frequency\ Noise = \begin{cases} No, & \text{if 50 ms} < \text{all widths} < \text{300 ms} \\ Yes, & otherwise \end{cases} \tag{2.1}$$

In order to obtain similar results to the ones obtained in [32], in this study the same ECG window of $10s$ has been considered, such as the same thresholds have been considered to classify the ECG segment as noisy or not. Furthermore, each ECG recording is split into a series of 10-second segments without overlapping, and each segment is then labelled with

the corresponding percentage of noise in that particular segment, by simply computing:

$$Percentage\ of\ Noise_i = \frac{\#Noisy\ samples_i \cdot 100}{\#Signal\ lenght}$$
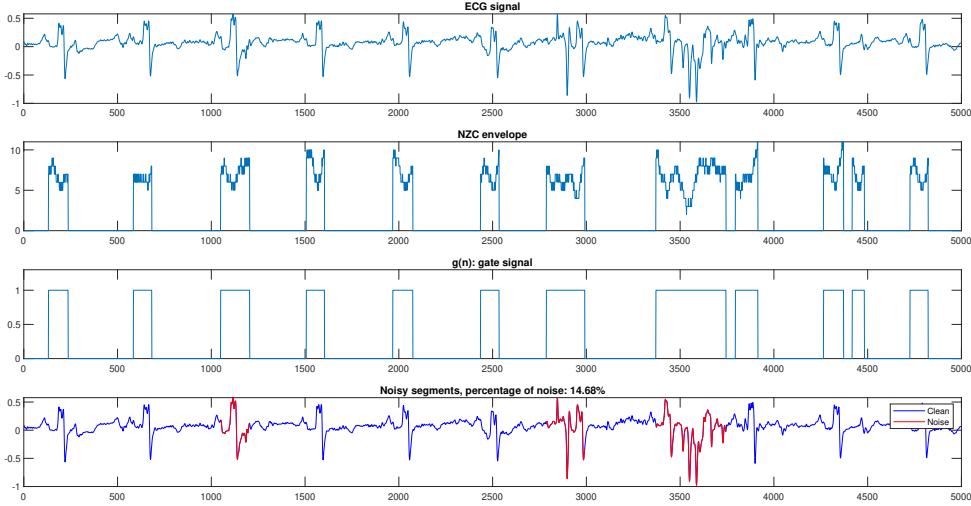
Figure 2.3: Detecting the presence of the noise from the gate signal $g[n]$. In the first row there is the original ECG signal. In the second row the NZC envelope is plotted. From the NZC envelope the gate signal (third row) is obtained. If the width of the gate signal is less than 50 ms or bigger than 300ms, the portion of the ECG signal is labelled as noise (represented in red in the fourth row).

A complete example of the application of the CEEMD algorithm for a 10-second ECG segment is the following:

- The original signal is decomposed in its IMFs, as represented in Figure 2.4

- $h[n]$, $c[n]$, $b[n]$ are derived from the IMFs, as shown in Figure 2.5

- Starting from $h[n]$, the NZC envelope and the gate signal are computed (Figure 2.6)

- At that point, when Equation 2.1 is verified, the noise is detected, as shown in Figure 2.7
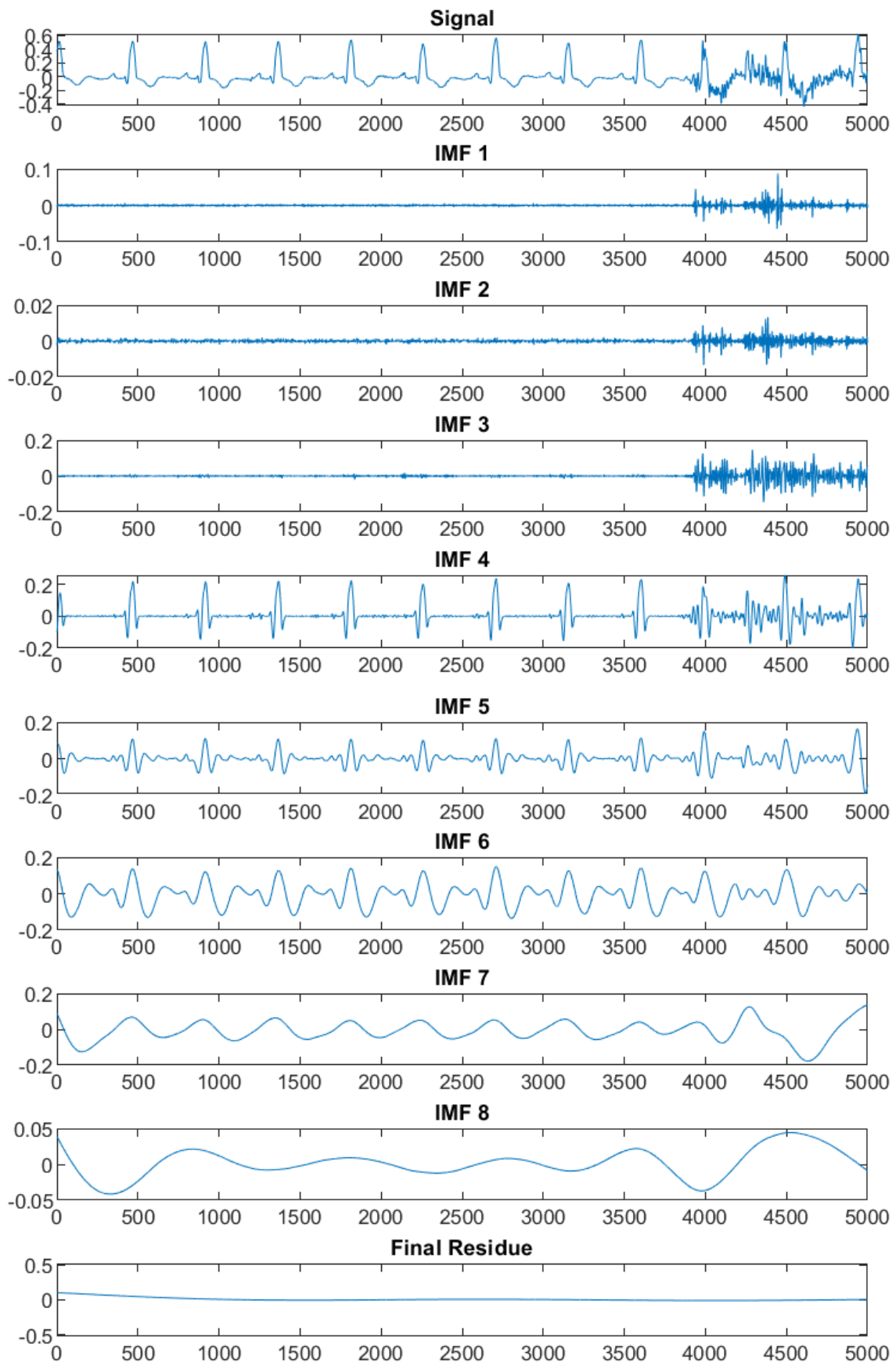
Figure 2.4: Decomposition of the original signal in its IMFs.
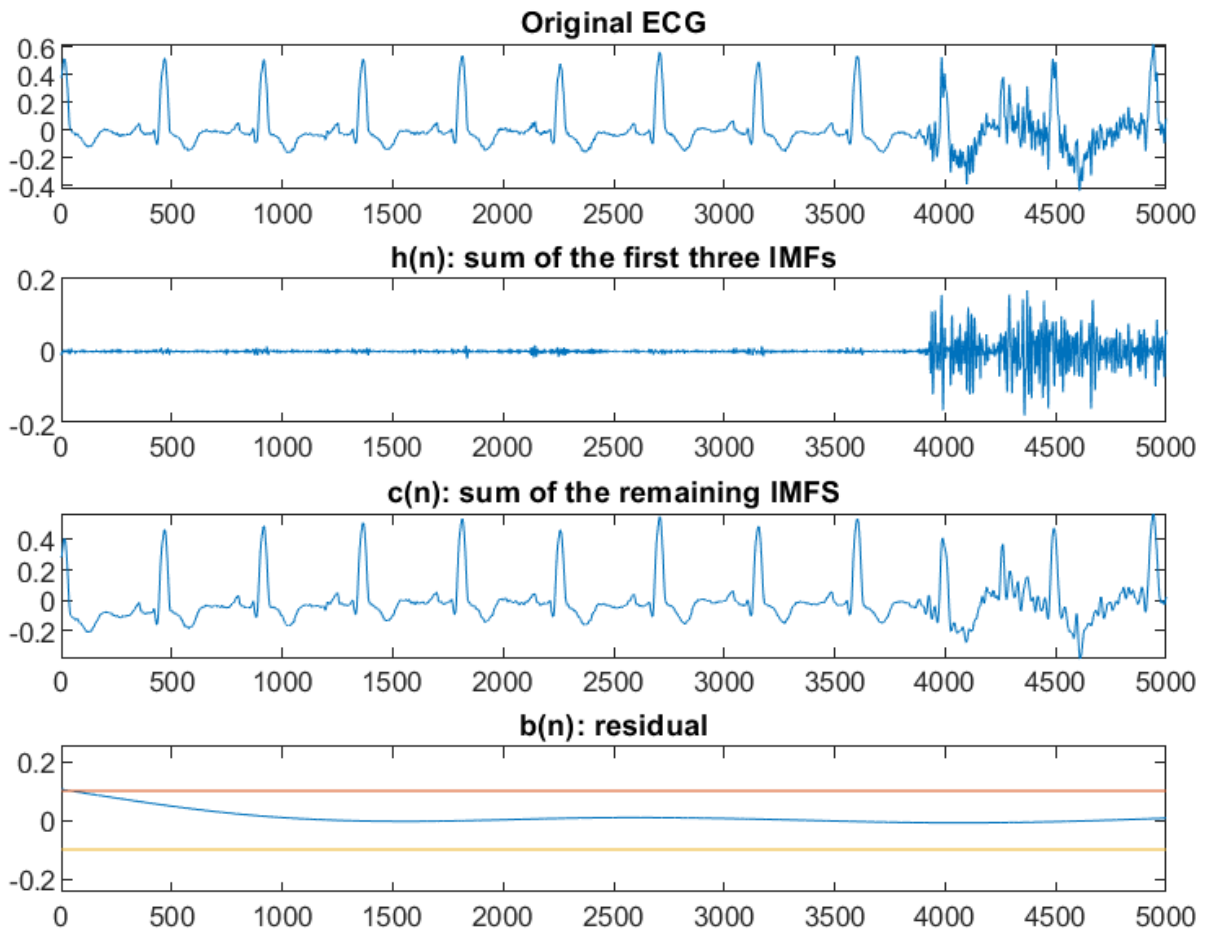
Figure 2.5: Decomposition of the original signal in its IMFs.
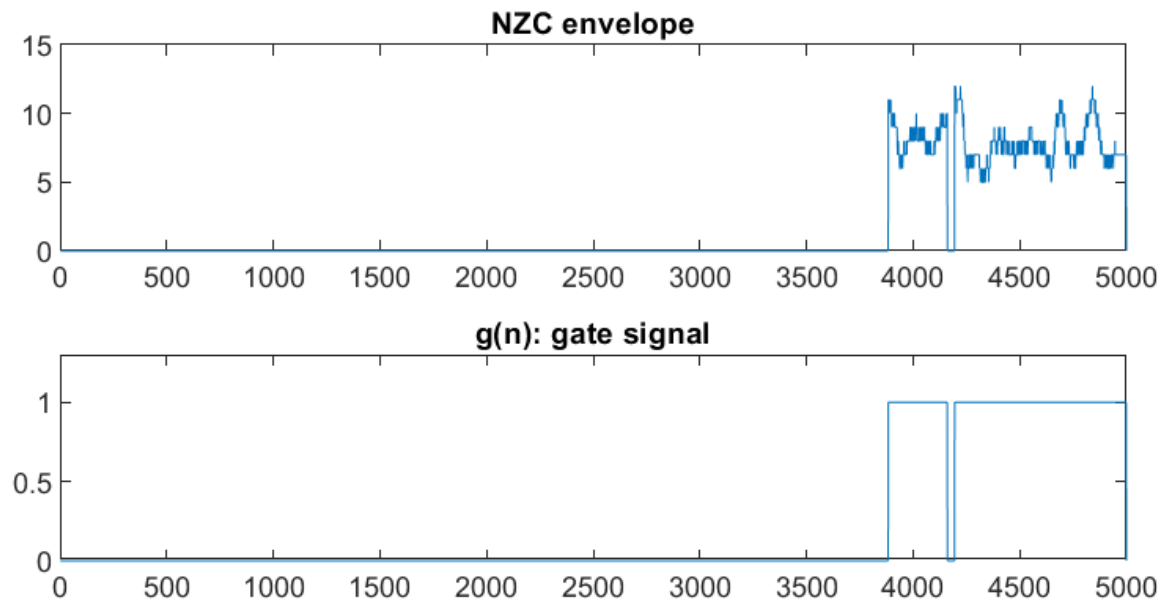
Figure 2.6: NZC envelope and gate signal are derived from the $h[n]$ function.
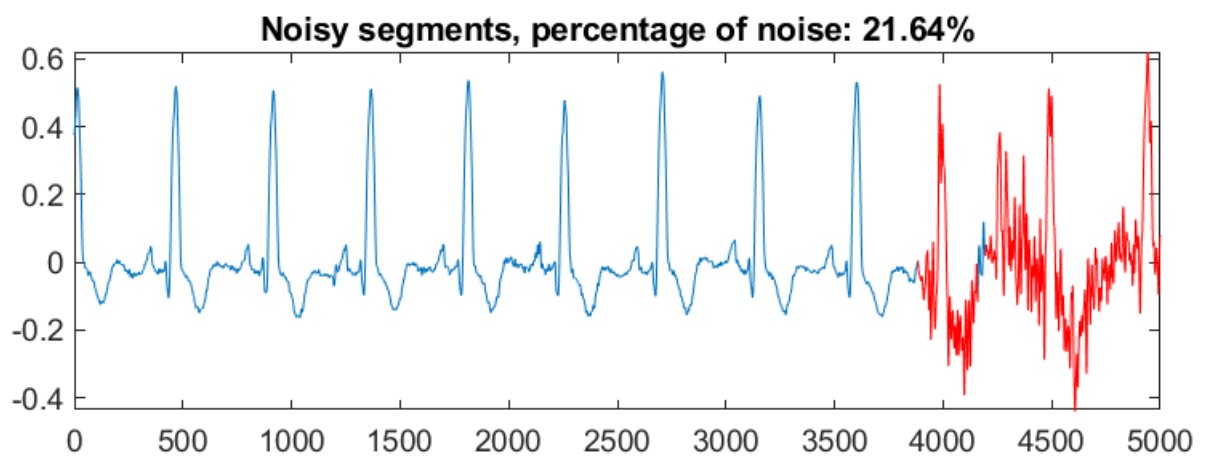
Figure 2.7: The noisy part of the segments detected by the CEEMD algorithm are high-lighted in red.

2.3. $\mathcal{V}$-index

The $\mathcal{V}$-index is an ECG-based estimator of the standard deviation of ventricular myocytes' repolarization times across the entire myocardium, obtained from multi-leads surface ECG [16]. It is estimated by considering multiple beats under a stable heart rate.

The electrophysiological model of the surface ECG put forward by van Oosterom [35] and a statistical model of the myocytes' repolarization timings [16] are combined to create the $\mathcal{V}$-index. Van Oosterom demonstrated how a weighted sum of the myocytes' transmembrane potentials can be used to model the structure of the T-wave on the surface ECG in a single beat. A weighted sum of a single function $T_d(t)$ (the so-called *dominant T-wave* [36]) and its derivatives can be used to approximate the multi-lead surface ECG in a first approximation since the repolarization phase of the action potential is comparable across myocytes at a particular heart rate, as follows:

$$\Psi(t) \approx -A\Delta\rho T_d(t) + \frac{1}{2}A\Delta\rho^2 \dot{T}_d(t)$$

where Ψ is the $[L \times 1]$ ECG, with L being the number of leads, the terms w_1, w_2 are $[L \times 1]$ vectors of lead factors, A is a patient-dependent $[L \times M]$ transfer matrix accounting for the contribution of each node to the L-leads electrocardiographic recording in $\Psi(t)$ and $\Delta\rho = [\Delta\rho_1(k), \Delta\rho_2(k), ..., \Delta\rho_M(k)]^T$ is a vector of repolarization delays.

Sassi and Mainardi [16] proposed a model for the repolarization delay $\Delta\rho_m$ for each cell m, obtained by dividing the myocardium in M cells, as follows:

$$\Delta\rho_m(k) = \rho_m(k) - \overline{\rho(k)} = \theta_m + \varphi_m(k)$$

where $\overline{\rho(k)}$ is the average repolarization time $\overline{\rho(k)} = \frac{1}{M}\sum_{m=1}^{M}\rho_m(k)$ in the single beat k over the set of M cells; θ_m models the spatial variability of the repolarization times for a given subject at a given heart rate; $\varphi_m(k)$ describes differences in repolarization times which are observable among successive beats (the temporal variability of the repolarization times). An estimate $\mathcal{V}_i$, where i represents the i_{th} lead, of the standard deviation of θ_m is given by

$$\mathcal{V}_i = \frac{std[w_2(i)]}{std[w_1(i)]} \approx \left(\sum_{m=1}^{M}\frac{\theta_m^2}{M}\right)^{1/2} = s_\theta \tag{2.2}$$

In order to compute the $\mathcal{V}$-index the following steps, similar to the ones used in [19], were followed:

- The CEEMD algorithm illustrated in 2.2.2 was used to scan the entire 24h ECG recording in lead I, II and V2.

- 10-minute clean segments were extracted from the 24h ECG. The segments were considered clean if respecting the following criteria:

  - At least 20% of the 10-minute segment, split into portions of 10-second sub-segments, is labelled as clean by the CEEMD algorithm

  - The 10-minute segment is considered clean in all three leads.

- By subtracting a horizontal line estimated as [18] (obtained by averaging the ECG samples contained in the TP segments, roughly identified as the mode of the ECG's amplitude distribution), the isoelectric line for each lead individually was roughly set to $0mV$.

- On lead II, beats were identified using an ad-hoc Pan-Tompkins detector implementation, and then, using a cross-correlation-based technique, fiducial points were retrieved using a QRS template to align the beats.

- The average cross-correlation between the aligned QRS complexes and the QRS template was used to evaluate the lead quality. Leads were deemed to be of sufficient quality and subjected to additional analysis if their average cross-correlation was higher than 0.8.

- Values for $T_d(t), w_1$ and w_2 are estimated for each T-wave of each normal beat, using the numerical approach described in [16].

- The sample standard deviations for the values of $w_1(i)$ and $w_2(i)$ acquired on successive beats are computed for each high-quality lead i.

- The $\mathcal{V}_{HL}$-index, on each high-quality lead (HL), is computed using Equation (2.2)

- The consistency of the $\mathcal{V}$-index is increased by averaging the $\mathcal{V}$-index computed in every single high-quality lead:

2.4.   Cox proportional-hazards model

By far, the most used method for modelling the connection between variables and survival or other censored outcome is the Cox proportional hazards model [37]. The following steps are illustrated by Therneau and Grambsch in detail in [38].

Considering X_{ij} as the j_{th} covariate of the i_{th} person, with $i = 1...n$ and $j = 1...p$ and thinking about the set of covariates as forming a $n \times p$ matrix, each row X_i of the matrix is the vector of covariate for the i_{th} person.

The hazard for the individual i is specified by the Cox model as follows:

$$\lambda_i(t) = \lambda_0(t)e^{X_i\beta}$$

where λ_0 represents the baseline hazard, an undefined nonnegative function of time, and β is a $p \times 1$ column vector of coefficients. The model specifies how the baseline hazard of patient i changes with the variables X_i.

The hazard ratio for two subjects with fixed covariate vectors X_i and X_j, computed as:

$$\frac{\lambda_i(t)}{\lambda_j(t)} = \frac{\lambda_0(t)e^{X_i\beta}}{\lambda_0(t)e^{X_j\beta}} = \frac{e^{X_i\beta}}{e^{X_j\beta}}$$

is constant over time, and for this reason, the model is also known as the proportional hazards model.

The partial likelihood (PL) function introduced by Cox [37], can be used to estimate the set of coefficients β. For untied failure time data it has the form

$$PL(\beta) = \prod_{i=1}^{n}\prod_{t\geq 0}\left\{\frac{Y_i(t)r_i(\beta,t)}{\sum_j Y_j(t)r_j(\beta,t)}\right\}^{dN_i(t)}$$

where $r_i(\beta,t)$ is the risk score for subject i, $Y_i(t)$ is the indicator function that subject i is still under observation at time t (1 in this case, 0 otherwise) and $N_i(t)$ is the number of observed events in [0, t] for subject i. The log PL can be written as a sum:

$$l(\beta) = \sum_{i=1}^{n}\int_0^\infty \left[Y_i(t)X_i(t)\beta - \log\left(\sum_j Y_j(t)r_j(t)\right)\right]dN_i(t)$$

The PL can be regarded as a likelihood for purposes of asymptotic inference even if it is not, in general, a likelihood in the sense of being proportional to the probability of an

observed dataset. By differentiating the log PL with respect to β, the score vector $U(\beta)$ is obtained, in the form of a $p \times 1$ vector:

$$U(\beta) = \sum_{i=1}^{n} \int_{0}^{\infty} [X_i(s) - \bar{x}(\beta, s)] \, dN_i(s)$$

where $\bar{x}(\beta, s)$ is simply a weighted mean of X, over those observations still at risk at time s,

$$\bar{x}(\beta, s) = \frac{\sum Y_i(s) r_i(s) X_i(s)}{\sum Y_i(s) r_i(s)}$$

with $Y_i(s) r_i(s)$ as the weights.

Once the score vector $U(\beta)$ is obtained, the maximum PL estimator is found by solving the PL equation:

$$U(\hat{\beta}) = 0$$

obtaining a solution $\hat{\beta}$ which is consistent and asymptotically normally distributed.

2.5.   Cosinor Analysis

In order to investigate if the $\mathcal{V}$-index follows a cyclic rhythm, a further investigation using the cosinor model [39] has been conducted. The cosinor model, which is a technique for modelling cyclical variation, fits a cosine curve to data using a regression model. The Least Squares process is used to fit data, which is a technique helpful in curve-fitting issues when it is desired to find a functional form that best matches a given collection of measurements. It is possible to write the regression model for a single-component cosinor as

$$y(t) = M + A\cos\left(\frac{2\pi t}{\tau} + \phi\right) + e(t)$$

where M is the mesor, A is the amplitude, ϕ is the acrophase (a measure of the time of peak reoccurring in each cycle), $e(t)$ is the error term and τ is the period, which has been imposed to be of 24 hours.

The least squares method's guiding concept is to minimize the residual sum of squares (RSS), which is the total of the squared differences between measurements Y_i (obtained at times t_i, $i = 1, 2, ..., N$) and the values estimated from the model at corresponding times $\hat{Y}_i$:

$$RSS = \sum_{i=1}^{N} (Y_i - \hat{Y}_i)^2,$$

where $\hat{Y}_i$ can be rewritten as:

$$\hat{Y}_i = \hat{M} + \hat{\beta}x + \hat{\gamma}z + e(t)$$

where

$$x = \cos\left(\frac{2\pi t}{\tau}\right)$$

$$z = \sin\left(\frac{2\pi t}{\tau}\right)$$

Computing the first-order derivative with respect to each parameter and imposing them equal to zero, the normal equations are obtained and used to estimate M, β, and γ. Starting from these estimations, estimates of the amplitude and acrophase can be computed using:

$$\hat{A} = (\hat{\beta}^2 + \hat{\gamma}^2)^{\frac{1}{2}},$$

$$\hat{\phi} = \arctan(-\frac{\hat{\gamma}}{\hat{\beta}}) + K\pi$$

where K is an integer value. The null hypothesis H_0 (no rhythm is present) is rejected, and so the model is statistically significant, when

$$F > F_{1-\alpha}(2, N-3)$$

where N is the number of samples and F is the result of the F-test, computed as

$$F = \frac{\frac{MSS}{2}}{\frac{RSS}{N-3}}$$

being α the specified probability threshold, 2 and $N-3$ the numbers of degrees of freedom of the model ($k = 3$ $parameters - 1$) and of the error term ($N - k - 1$) and MSS the Model Sum of Squares, computed as

$$MSS = \sum_{i=1}^{N}(Y_i - \overline{Y_i})^2$$

where $\overline{Y_i}$ is the mean of the observations.

3 | Results

3.1. Population

Table 3.1 shows differences in the characteristics of the patients, divided into two groups: alive and CV dead patients.

Variable	Alive	CV Dead	p-value
Number of patients	325	55	
Age (years), mean ± std	63.82 ± 10.27	70.36 ± 9.37	<0.0001
Gender (M)	267 (82%)	46 (84%)	0.78
LVEF (%), mean ± std	32.81 ± 8.42	29.67 ± 7.7	<0.01
NSVT	130 (40%)	36 (65%)	<0.0001
Creatinine (mg/dL), mean ± std	1.11 ± 0.32	1.54 ± 0.93	<0.0001
Sodium (mEq/L), mean ± std	140.1 ± 3.93	140.11 ± 3.8	0.98
Potassium (mEq/L), mean ± std	4.45 ± 0.48	4.57 ± 0.54	0.09
Bilirubin (mg/dL), mean ± std	0.76 ± 0.37	0.75 ± 0.3	0.38
NYHA class III-IV	59 (18%)	18 (33%)	0.02
ACE	305 (94%)	52 (94%)	0.84
Beta-blockers	235 (72%)	28 (51%)	<0.01
Diuretics	266 (82%)	54 (98%)	<0.01
Digitalis	68 (21%)	18 (33%)	0.05
Nitrates	99 (30%)	26 (47%)	0.01
Amiodarone	44 (14%)	16 (29%)	<0.01
Ischaemic cardiomyopathy	157 (43%)	35 (64%)	0.03

Table 3.1: Demographic and clinical characteristics in the entire population.

The two groups were compared for each variable, using the t-test or Wilcoxon test for numerical variables and χ^2 for categorical variables.

CV dead patients were older (see Figure 3.1), with higher values in creatinine, and smaller values in LVEF. Also, they have a higher incidence of NSVT, a more advanced NYHA class and had less BBL treatment. No significant difference is related to the gender of the patients.
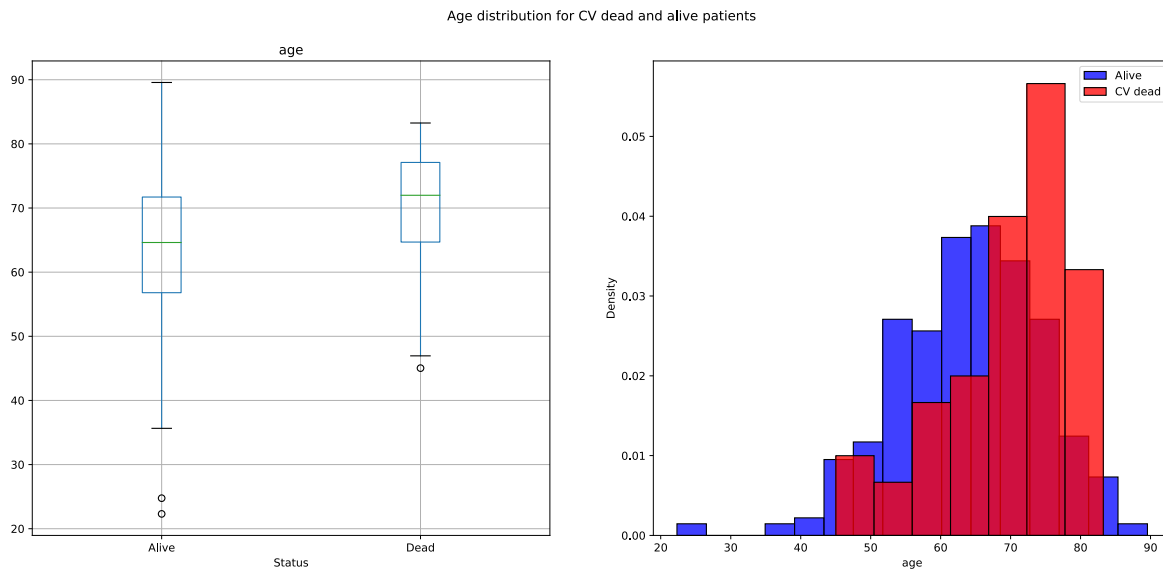
Figure 3.1: Age distribution for survived and dead patients. The two distributions are statistically different ($p < 0.05$).

In Figure 3.2 are illustrated the boxplots of the age, in relation to the status (dead or not) and the gender. The distribution of the age for dead males is statistically different ($p < 0.001$) with respect to survived males, such as the distribution of the age for dead females is statistically different ($p < 0.05$) with respect to survived females. Differences between the age distribution for dead females and dead males are not statistically significant ($p > 0.05$).
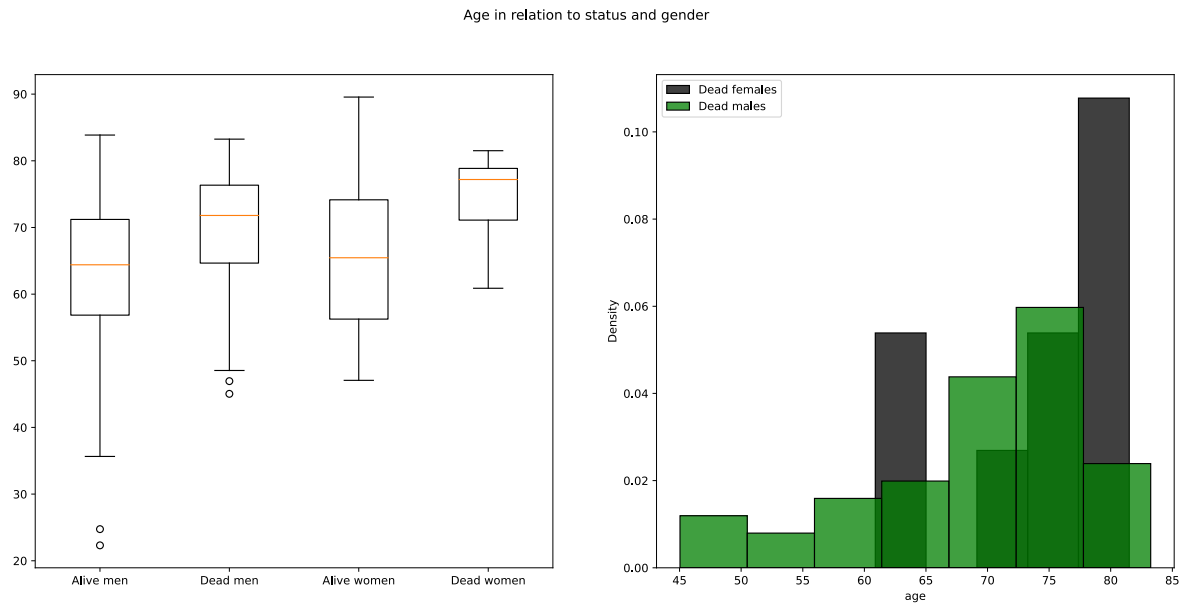
Figure 3.2: On the left, the boxplots of the age distribution of mixed status and gender. On the right, is a comparison of the age distribution for dead males and dead females.

3.2. Noise Detection

Final demonstrations of the CEEMD algorithm, described in Section 2.2.2, are shown in Figure 3.3 for noise-free ECG segments (on the left) and for noisy ECG segments (on the right). The algorithm is able to identify sudden swings in the signal and discern them from the regular ECG, localizing with sufficient precision the noisy part of the segment. The CEEMD algorithm was used to scan the entire 24h ECG recordings to obtain the noise-free 10-minute segments, such that $\mathcal{V}$-index could be robustly computed. The distribution of the number of 10-minute segments available for each patient in each visit is illustrated in Figure 3.4. In visit 2 the number of available clean segments ranged between 0 and 140, with 65 ± 38 segments for patient, in visit 4 63 ± 38 segments in a range of 0-133, while in visit 6 66 ± 38 segments from the minimum of 0 to the maximum of 140.
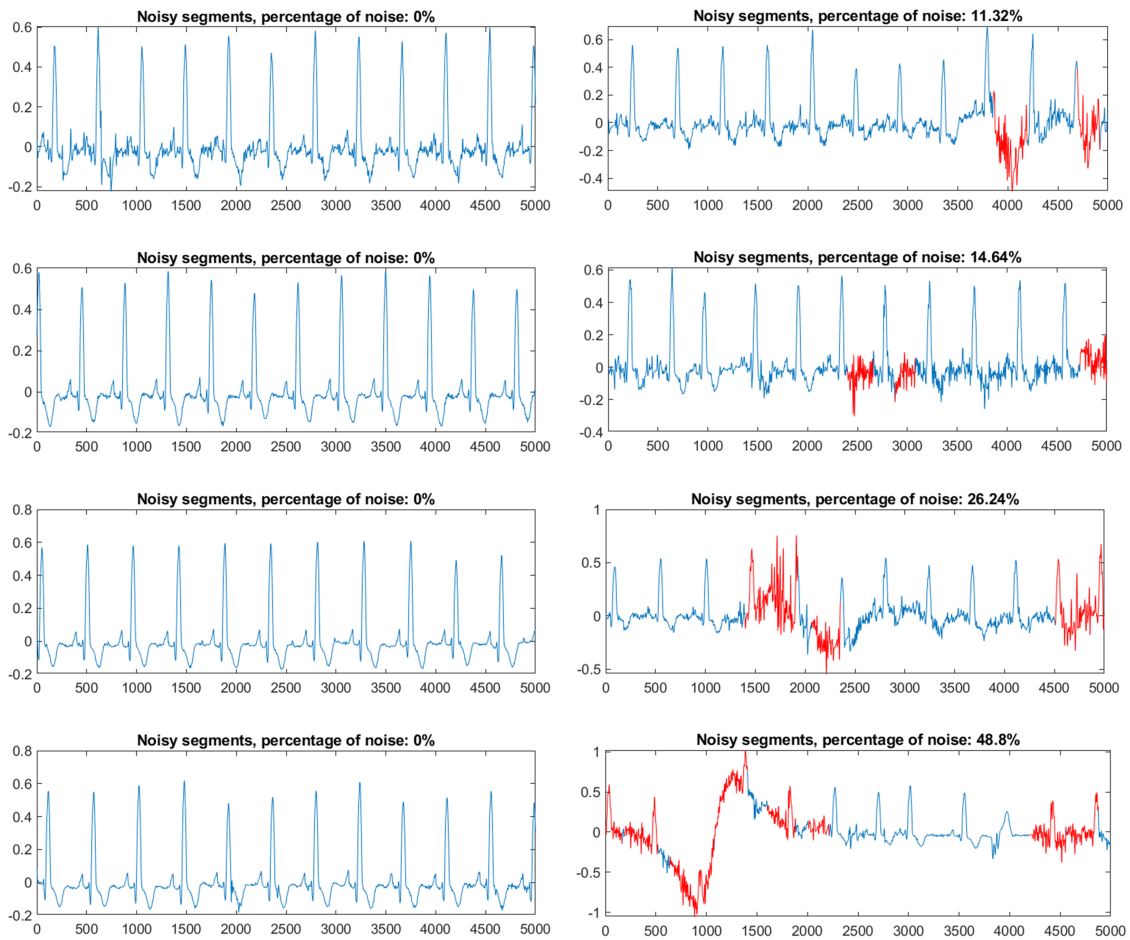
Figure 3.3: Examples of application of the CEEMD algorithm. Performances of the algorithm are shown on the left for clean segments, while on the right for progressively noisier segments. Red lines represent the portion of the segment labelled as noise by the algorithm.
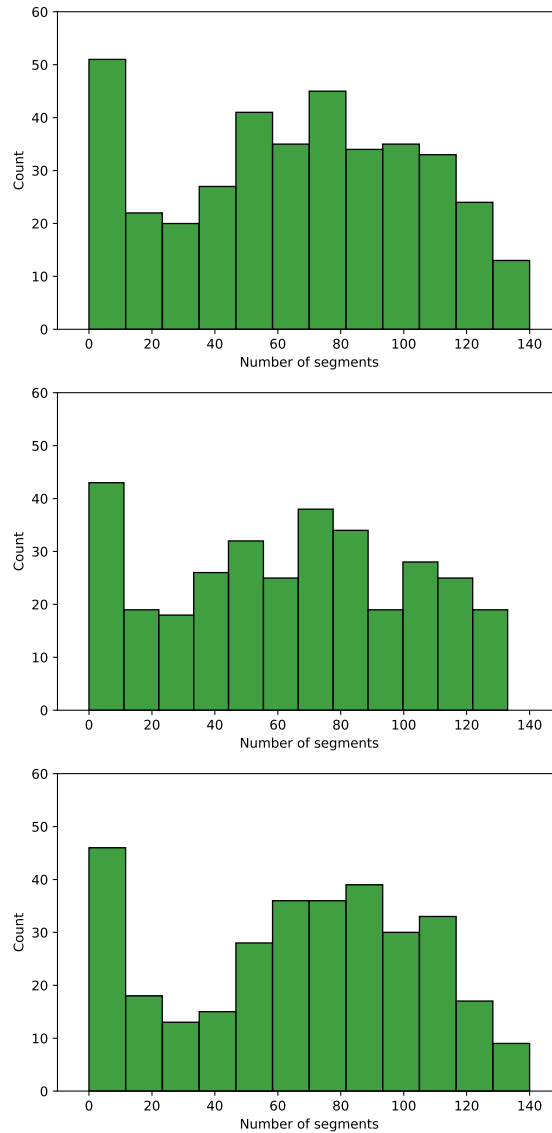
Figure 3.4: Number of 10-minute noise-free segments in which $\mathcal{V}$-index has been computed, for each visit.

Further analyses have been made in order to check if the number of segments taken into consideration for the alive patients was different from the ones computed for CV dead patients, so introducing a bias in the models. Fig 3.5 shows the distributions for CV dead and alive patients in each visit. A comparison between the two groups for each visit has been made using the Wilcoxon test, resulting in non-significant differences for each visit (Visit 2: $p = 0.86$, Visit 4: $p = 0.08$, Visit 6: $p = 0.18$).
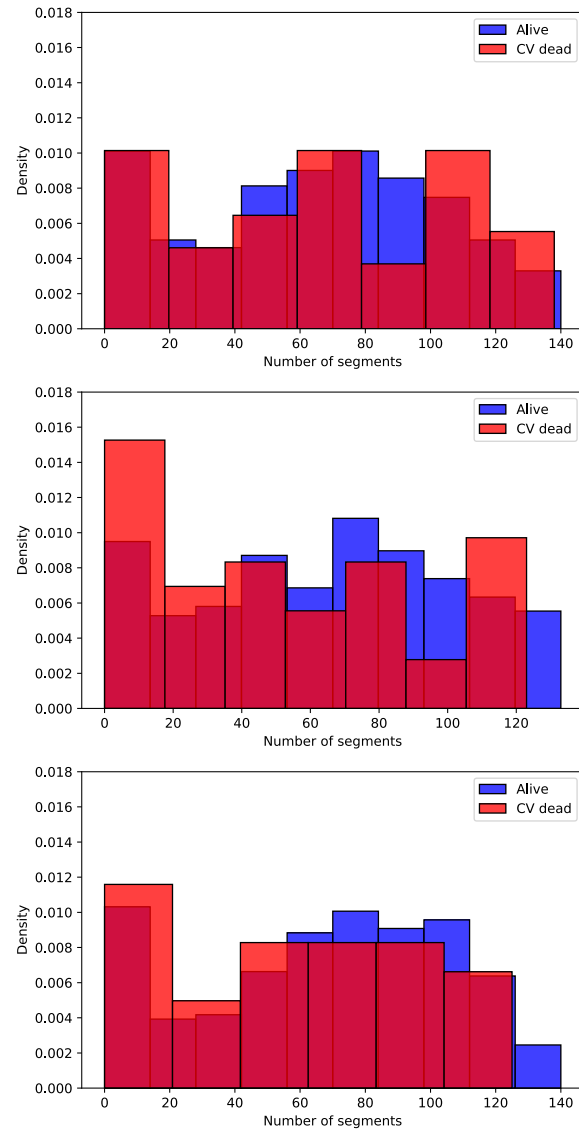
Figure 3.5: Distributions and boxplots of the number of segments on which $\mathcal{V}$-index was computed for CV dead and alive patients, for each visit.

3.3. $\mathcal{V}$-index

The number of patients for which the $\mathcal{V}$-index was computed in at least one segment, is illustrated in Table 3.2, resulting in 365 patients with at least one $\mathcal{V}$-index value in visit 2, while 307 and 301 patients in visit 4 and 6, respectively. The number of available patients and available ECG recordings, and consequently the number of patients on which has been possible to compute at least one $\mathcal{V}$-index value, changed during the follow-up: of the 380 (308 survivors, 72 non-survivors of which 55 CV dead) patients present in the first visit, 5 of them died for CV reasons between visits 2 and 4. Of the 375 (308 survivors, 67 non-survivors) patients that were still alive, 326 underwent the visit 4 (270 survivors patients, while 56 non-survivors, of which 41 died for CV reasons). During visit 4 and visit 6, 14 patients died for CV reasons and 1 patient for other reasons. Of the 360 (308 survivors, 52 non-survivors) patients alive at the time of the last visit, 320 were ECG recorded (278 survivors, 42 the non-survivors, of which 29 died for CV reasons).

	Visit 2 (S-NS(CV))	Visit 4 (S-NS(CV))	Visit 6 (S-NS(CV))
Patients	380 (308 - 72 (55))	375 (308 - 67 (50))	360 (308 - 52 (36))
Recordings	380 (308 - 72 (55))	326 (270 - 56 (41))	320 (278 - 42 (29))
$\mathcal{V}$-index	365 (295 - 70 (53))	307 (253 - 54 (39))	301 (261 - 40 (27))

Table 3.2: The first row represents the number of survivor patients at the time of each visit. The second row represents the number of patients who underwent the ECG recording. The last row represents the number of patients for which $\mathcal{V}$-index was computed in at least one segment, for each visit.

The cosine function has been fitted for each patient for each visit. The number N of data points used to fit the cosine function is different for each patient, depending on the number of segments in which has been possible to compute the $\mathcal{V}$-index, as illustrated in Figure 3.4. Patients with less than 5 available $\mathcal{V}$-index have not been considered for the cosinor analysis. Examples of the behaviour of the $\mathcal{V}$-index during the day, along with cosinor fittings, are illustrated in Figure 3.6 for two patients. Computing the F-test to investigate if the circadian rhythm is present, in visit 2 247 (214 alive, 33 CV dead) out of 342 patients (293 alive, 49 CV dead), in visit 4 201 (172 alive, 29 CV dead) out of 292 patients (257 alive, 35 CV dead) and in visit 6 202 (185 alive, 17 CV dead) out of 287 patients (263 alive, 24 CV dead) follows a circadian rhythm.
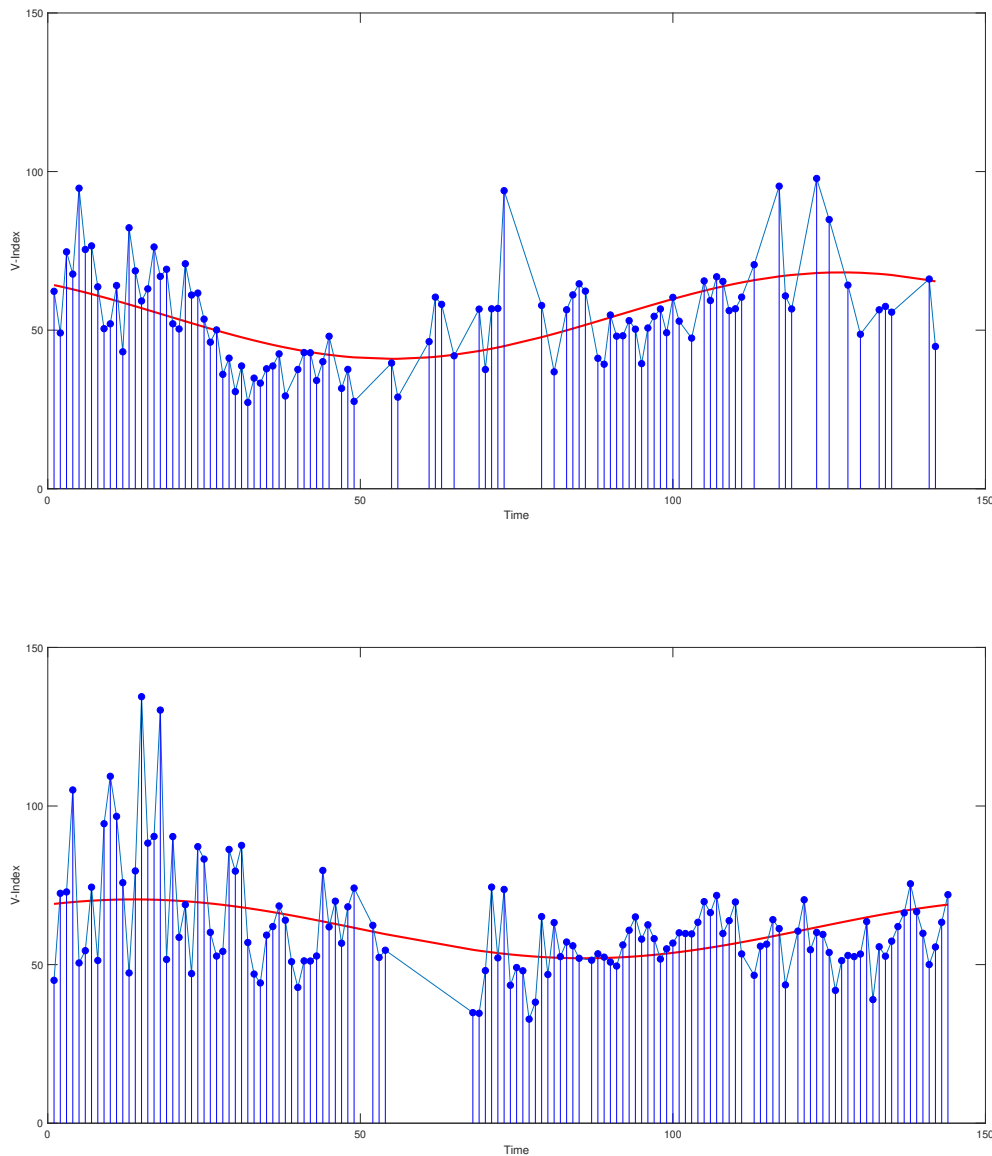
Examples of the Cosine Function fitting

Figure 3.6: On the X-axis, the 24 hours are divided into 144 ten minutes segments. Each blue dot represents a segment in which $\mathcal{V}$-index has been computed. The red line is the estimated cosine function.

The summary statistics for $\mathcal{V}$-index mesor and $\mathcal{V}$-index amplitude, computed through the steps illustrated in Section 2.5, are illustrated in Table 3.3. Figure 3.7 shows (on the left) the distribution of $\mathcal{V}$-index mesor of CV dead and alive patients in the three visits, while $\mathcal{V}$-index amplitude distributions are illustrated on the right. Additional investigations have been made to analyze if there were any differences between alive and CV dead patients. Distributions of $\mathcal{V}$-index mesor have been compared using the single tail Wilcoxon test,

showing significant differences in visit 2 ($p = 0.04$) while not in the other visits ($p = 0.18$, 0.31 respectively). The comparison among $\mathcal{V}$-index amplitude distributions, also in this case made with the single tail Wilcoxon test, does not show any significant differences in all three visits ($p = 0.36, 0.10, 0.23$ respectively).

Variable	Entire population	Alive	CV dead
$\mathcal{V}$-index mesor, v2	31.56 (23.68-41.55)	30.89 (23.07-40.90)	34.82 (27.60-43.79)*
$\mathcal{V}$-index mesor, v4	31.29 (24.27-41.30)	31.10 (24.18-39.39)	35.03 (24.98-48.36)
$\mathcal{V}$-index mesor, v6	33.05 (26.41-42.23)	32.90 (26.19-42.23)	36.22 (30.48-42.34)
$\mathcal{V}$-index ampl., v2	6.09 (3.06-10.88)	5.84 (3.09-10.89)	6.97 (3.01-10.43)
$\mathcal{V}$-index ampl., v4	5.94 (3.20-10.78)	5.79 (3.17-10.07)	7.66 (3.75-11.87)
$\mathcal{V}$-index ampl., v6	6.49 (3.41-11.28)	6.34 (3.40-11.28)	7.14 (3.78-11.72)

Table 3.3: Median and 25th-75th percentile of $\mathcal{V}$-index mesor and $\mathcal{V}$-index amplitude, for each visit. ampl: amplitude; the symbol * represents a $p < 0.05$.
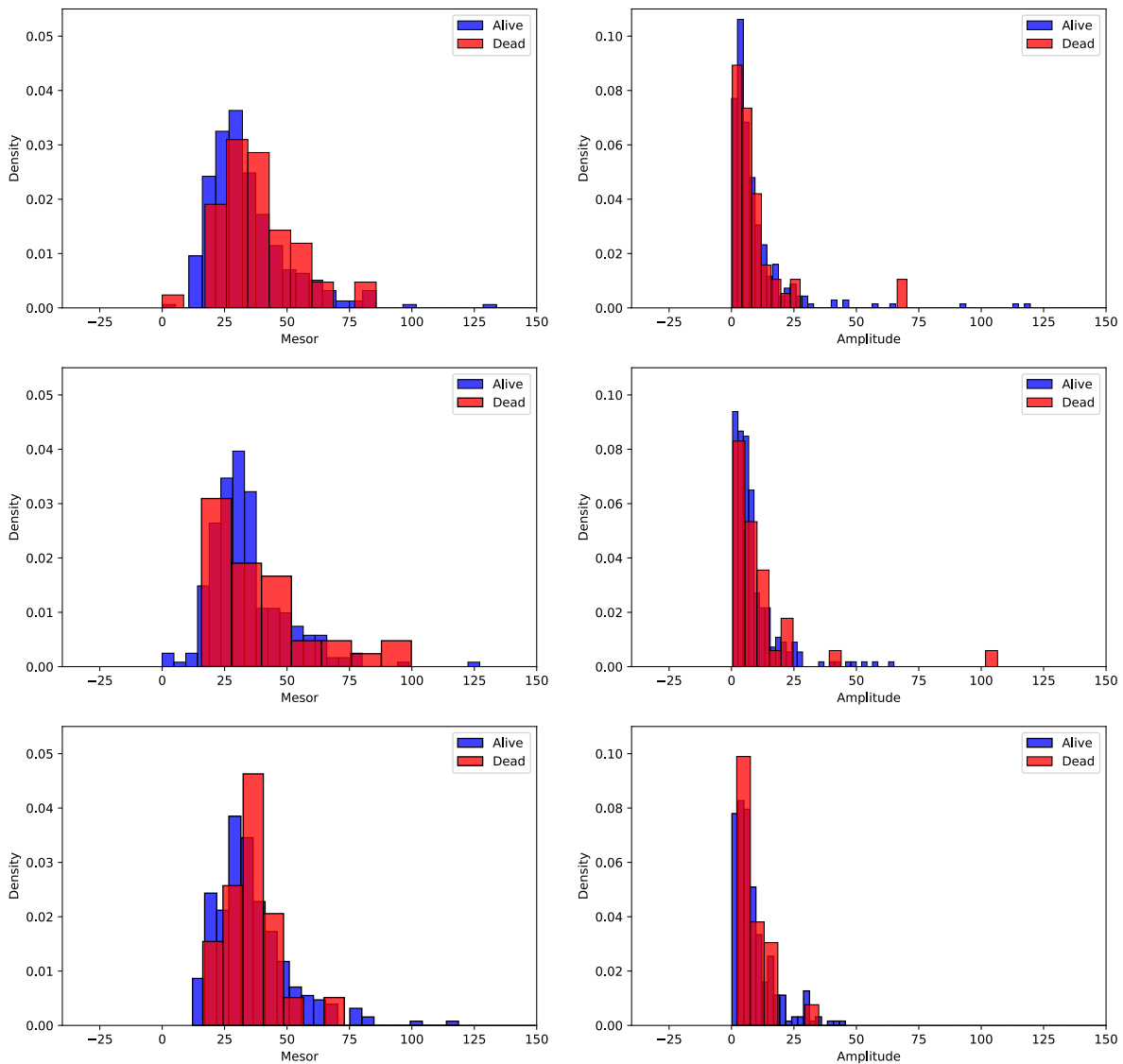
Figure 3.7: Mesor (on the left) and amplitude (on the right) distribution for dead and alive patients, for each visit.

An analysis of $\mathcal{V}$-index mean and $\mathcal{V}$-index median have been made in order to check if there were any differences between visits 2, 4 and 6, which distributions are represented in Fig 3.8, while the boxplots in Fig 3.9. Both for $\mathcal{V}$-index mean and $\mathcal{V}$-index median, comparison between visit 2 and 4, visit 2 and 6, and visit 4 and 6 have been made using the Wilcoxon test, showing no significant differences in any of the visits. An additional experiment has been made to compare the distribution of CV dead patients in the three visits, whose boxplots are represented in Figure 3.10 for $\mathcal{V}$-index mean and $\mathcal{V}$-index median in relation to the status. Also in this case, no significant differences have been found ($p > 0.1$).
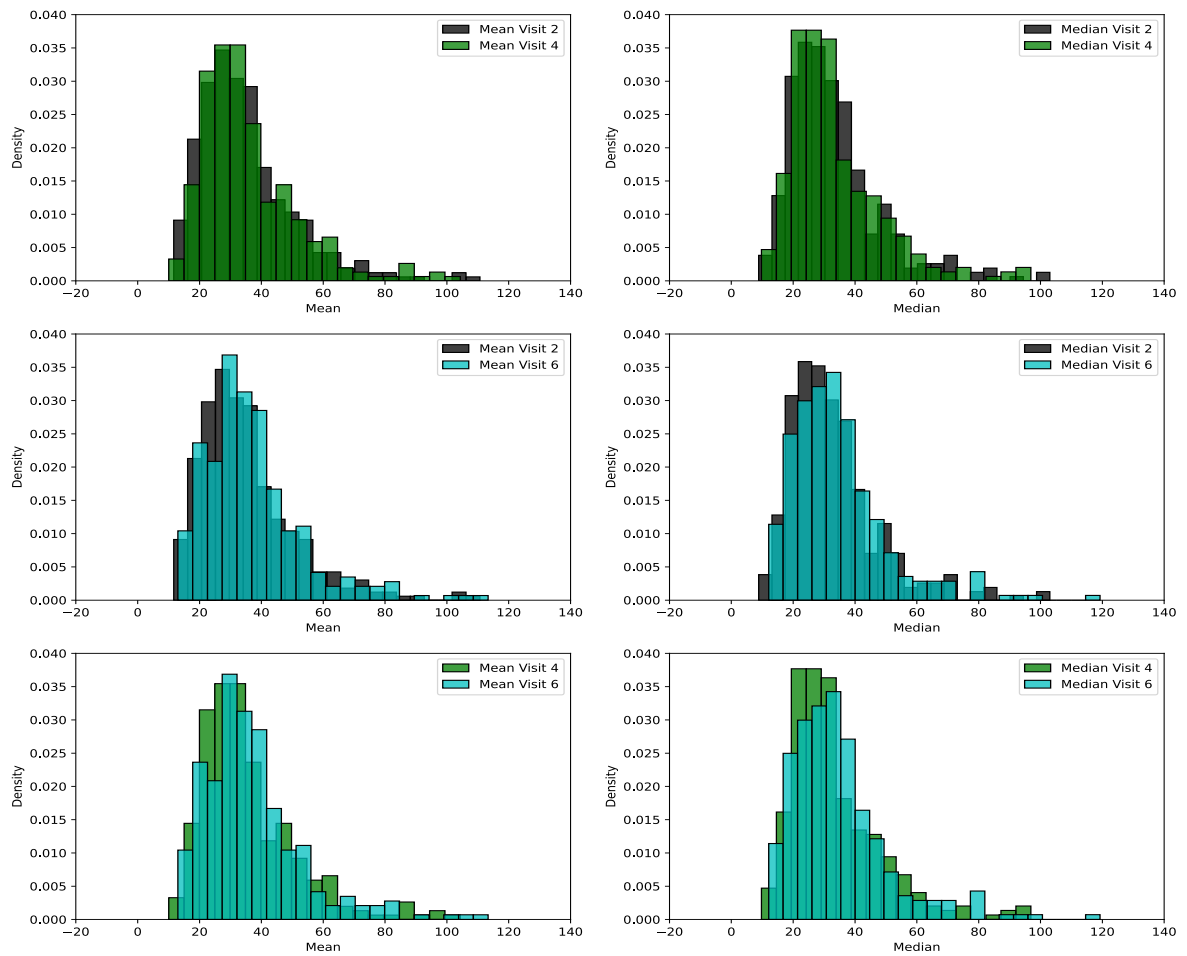
Figure 3.8: Comparison of the $\mathcal{V}$-index means (on the left) and medians (on the right) among the visits.
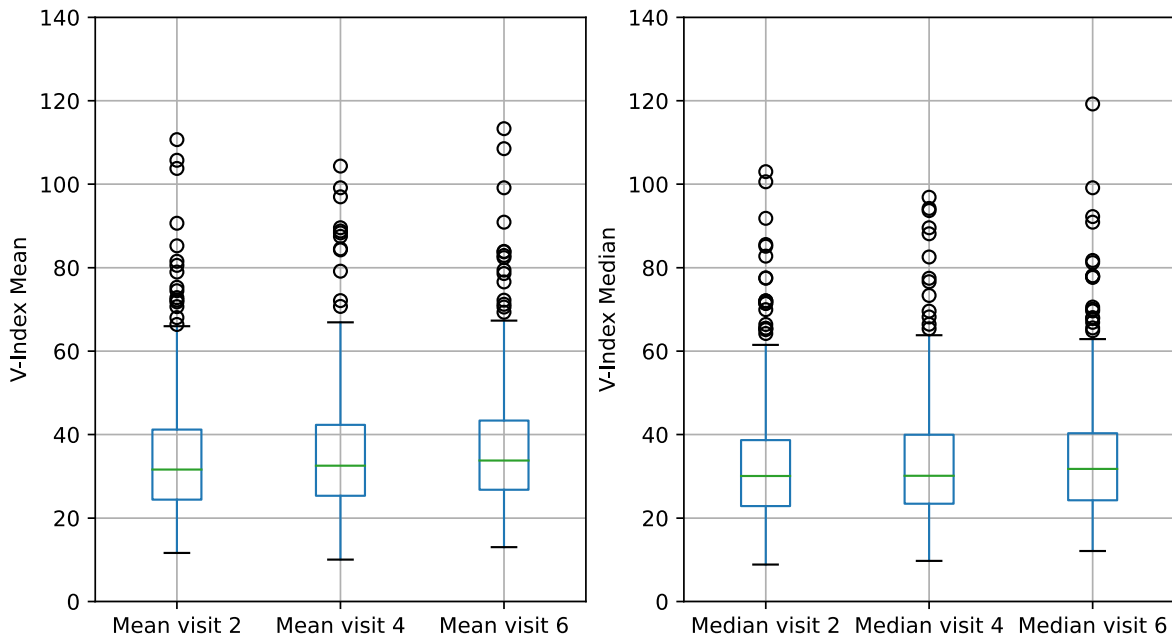
Figure 3.9: Boxplot for $\mathcal{V}$-index mean (on the left) and $\mathcal{V}$-index median (on the right), for each visit.
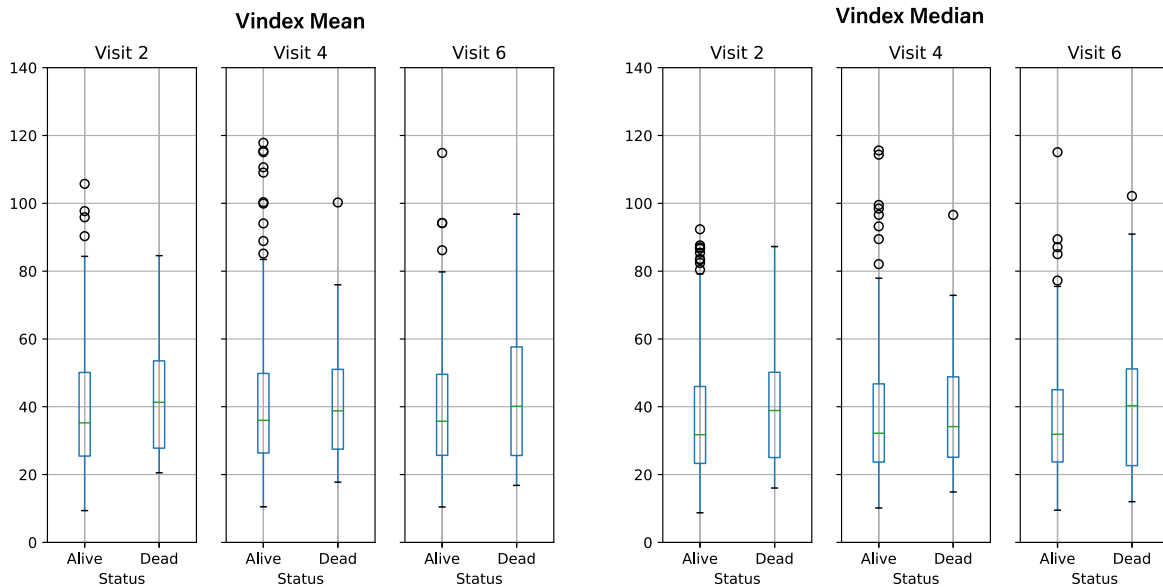
Figure 3.10: Distribution for the $\mathcal{V}$-index mean (on the left) and $\mathcal{V}$-index median (on the right), for each visit.

In order to have a statistic that summarizes $\mathcal{V}$-index values for each patient, mean, median, standard deviation (std), $\mathcal{V}$-index on the first available segment (all reported in Table 3.4)

and mesor and amplitude, have been used. The distributions of the $\mathcal{V}$-index values for CV dead and alive patients have been compared in each visit, trying to identify if the $\mathcal{V}$-index alone is able to separate the two groups. The distributions of the means of the $\mathcal{V}$-index values, represented in Fig. 3.11 (on the left), show significant differences between alive and CV dead patients in the first visit, while no differences are found in visit 4 and 6. Using the single tail Wilcoxon test for each visit the p-value was, respectively, 0.02, 0.07, and 0.29 for the 3 visits.

Variable	Entire population	Alive	CV dead
$\mathcal{V}$-index mean, v2	31.61 (24.43-41.21)	30.83 (23.88-39.81)	35.47 (27.53-46.90)*
$\mathcal{V}$-index mean, v4	32.57 (25.33-42.31)	31.99 (24.39-42.22)	34.97 (26.76-42.44)
$\mathcal{V}$-index mean, v6	33.77 (26.75-43.34)	33.46 (26.75-43.25)	37.25 (27.60-42.99)
$\mathcal{V}$-index median, v2	30.06 (22.86-38.67)	29.65 (22.51-37.42)	33.31 (25.68-46.02)*
$\mathcal{V}$-index median, v4	30.10 (23.41-39.93)	30.03 (23.36-39.21)	34.93 (25.39-41.75)
$\mathcal{V}$-index median, v6	31.77 (24.23-40.30)	31.38 (24.14-40.97)	34.75 (26.07-37.82)
$\mathcal{V}$-index std, v2	9.20 (6.40-14.03)	9.17 (6.14-13.94)	11.56 (7.03-14.26)
$\mathcal{V}$-index std, v4	9.60 (6.61-15.25)	9.48 (6.63-15.55)	9.76 (6.54-13.41)
$\mathcal{V}$-index std, v6	10.63 (7.05-16.40)	10.74 (7.30-16.04)	10.54 (6.38-17.08)
$\mathcal{V}$-index FS, v2	28.87 (20.49-39.55)	28.07 (20.34-38.26)	35.02 (26.47-50.03)*
$\mathcal{V}$-index FS, v4	28.64 (22.09-40.85)	28.17 (22.10-39.66)	35.27 (21.94-45.82)
$\mathcal{V}$-index FS, v6	29.15 (22.98-41.60)	28.75 (22.48-40.33)	34.67 (26.12-45.50)*

Table 3.4: Median and 25th-75th percentile of $\mathcal{V}$-index statistics, for each visit. v: visit; the symbol * represents a $p < 0.05$.
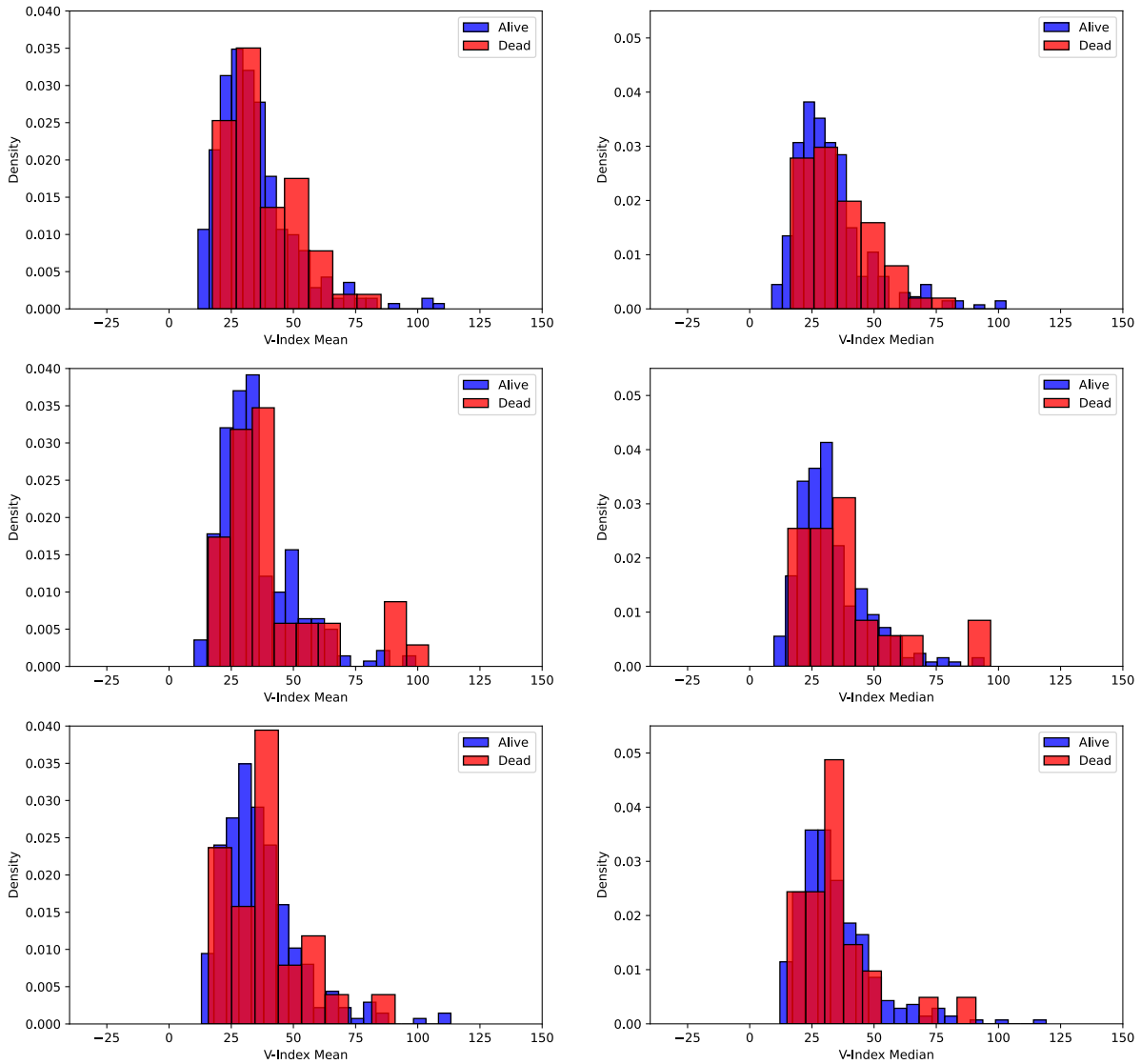
Figure 3.11: Distribution of the $\mathcal{V}$-index means (on the left) and medians (on the right), for each visit.

Considering the median as the summary statistic, whose distributions are shown in Fig. 3.11 (on the right), in the first visit there is a significant difference between the two groups, while differences in the other visits are not statistically significant, with a p-value of 0.02, 0.06 and 0.32 respectively. Distributions of $\mathcal{V}$-index standard deviation are shown in Figure 3.12 (on the right), with no significant differences in all the visits ($p = 0.07, 0.55, 0.54$). Considering the $\mathcal{V}$-index computed on the first noise-free segment of the day (shown in Figure 3.12 on the left), a statistical difference for the two groups is highlighted in visit 2 ($p < 0.01$) and visit 6 ($p = 0.02$) but not in visit 4 ($p = 0.06$).
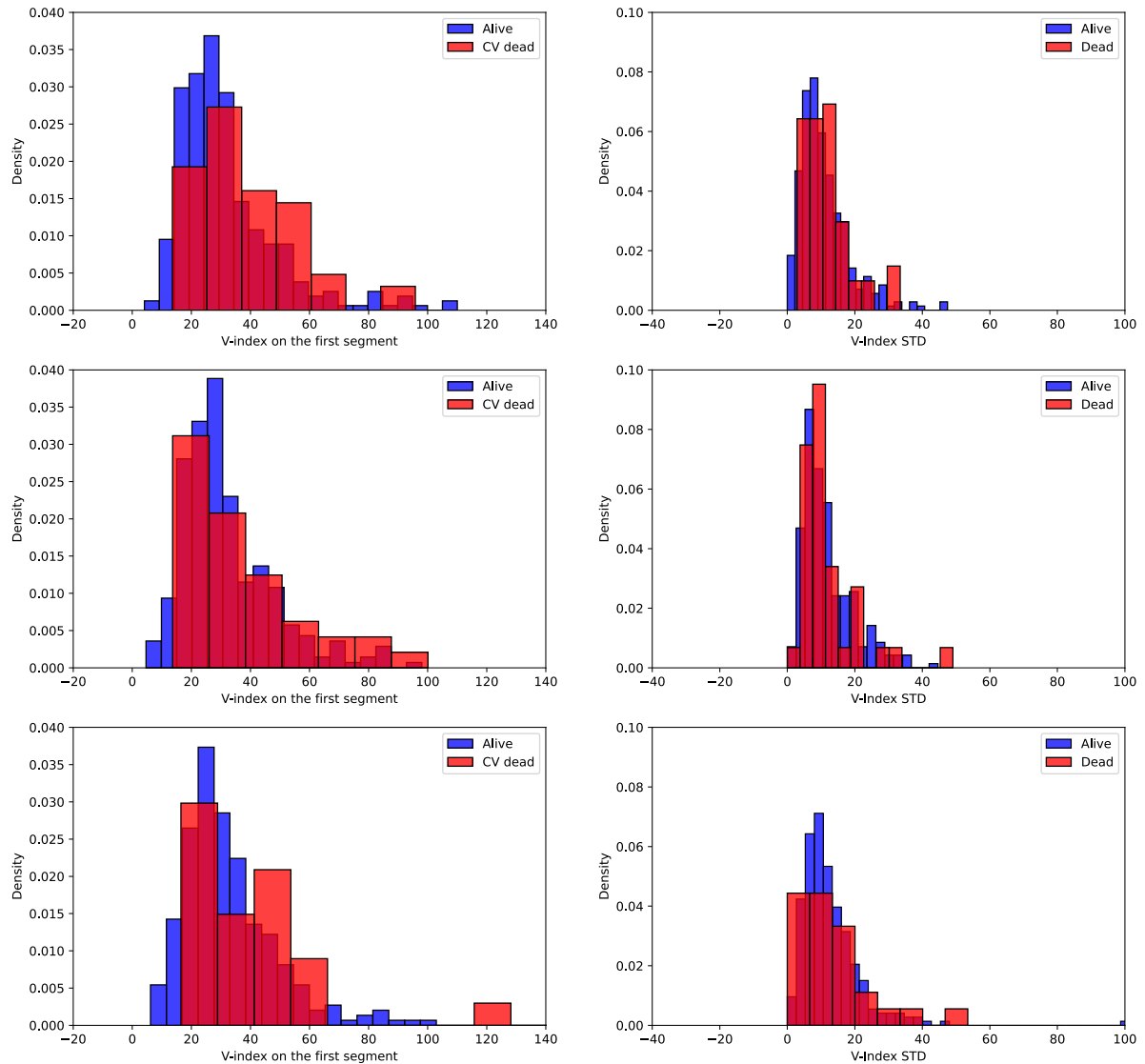
Figure 3.12: Distribution of the $\mathcal{V}$-index computed on the first available segment (on the left) and distributions of $\mathcal{V}$-index standard deviations (on the right), for each visit.

In addition to the statistics previously mentioned, a new signature has been computed starting from the cosinor analysis results. After computing a bivariate Cox model using mesor and amplitude, the coefficients (0.55 and 0.22 respectively) have been used in order to create this new variable, computed as follows:

$$Signature_{cosinor} = 0.55 \cdot Mesor_{cosinor} + 0.22 \cdot Amplitude_{cosinor}$$

The distributions of the $\mathcal{V}$-index signature are shown in Fig. 3.13. Distributions for alive and CV dead patients in visit 2 are statistically different (median 18.18 IQR (14.11-24.34)

vs median 21.48 IQR (15.88-26.64), $p = 0.04$) according to the single tail Wilcoxon test, while no differences are highlighted in visit 4 (median 18.35 IQR (14.44-24.35) vs median 21.66 IQR (14.84-29.07, $p = 0.08$) and visit 6 (median 19.66 IQR (15.82-25.43) vs median 21.30 IQR (18.06-25.64), $p = 0.15$).
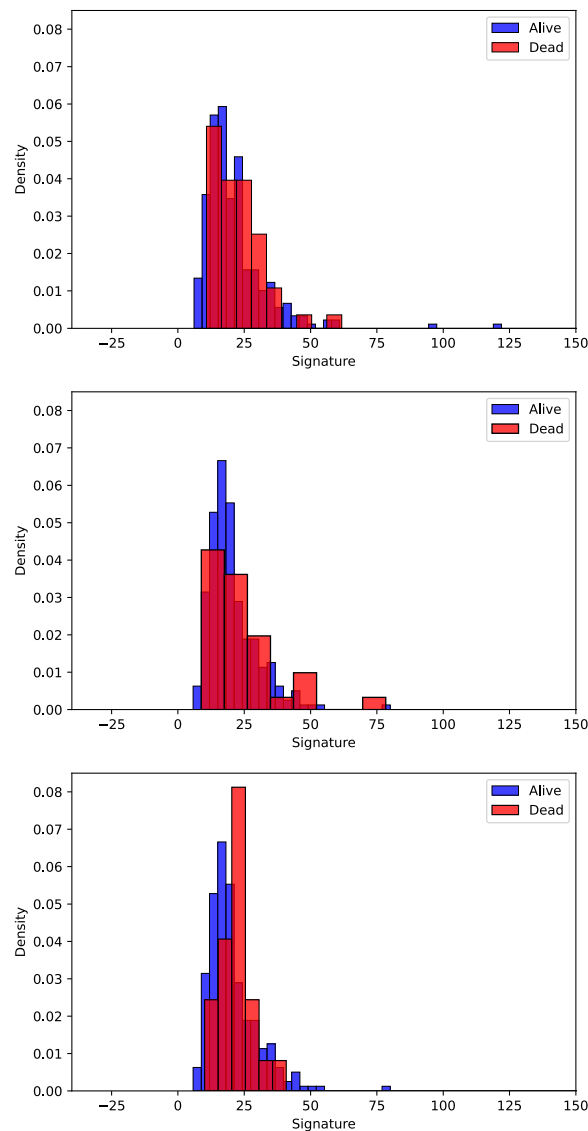
Figure 3.13: Distribution of the $\mathcal{V}$-index signature. Each row represents a visit.

Before fitting the data with the Cox model, different thresholds were found to dichotomize the numerical variables. To find these thresholds, the receiver operating characteristic (ROC) curve was used. The idea of a "separator" (or choice) variable is the base for the idea of a ROC curve. If the "criterion" or "cut-off" for positivity on the decision axis is altered, the frequency of positive and negative diagnostic test outcomes will change [40].

A ROC curve is produced by plotting TPR (true positive rate, sensitivity) versus FPR (false positive rate, 1-specificity) across various cut-offs. While sensitivity is computed as $\frac{TP}{TP+FN}$, specificity is computed as $\frac{TN}{TN+FP}$. When plotting the ROC curve, the most the curve is closer to the upper left corner (0 FPR, 1 TPR) the better the discriminant capabilities of the test. The performance of a diagnostic test that is no better than chance level, so a test that produces positive or negative results unrelated to the true status, is represented by a ROC curve that is on the diagonal line. The area under the curve (AUC) describes the intrinsic validity of diagnostic tests and it is a useful combination of sensitivity and specificity metrics.

The steps followed in order to find the best separating thresholds, related to the ability of the selected variable to discriminate between alive and CV dead patients, are the following:

- The numerical variable that needs to be binarized is selected

- An interval for the threshold is fixed between the minimum and the maximum value of the selected variable, along with a step

- For each threshold, the predicted outcome $\hat{y}$ is computed: if the value of the patient for the selected variable is greater than the threshold, the patient outcome is predicted as 1 (CV dead), 0 otherwise.

- TPR and FPR are computed comparing the true outcome y and the predicted outcome $\hat{y}$

- The threshold associated with the best FPR,TPR combination is selected.

In Figure 3.14 examples of the application of the previous steps are shown while finding the best threshold value for $\mathcal{V}$-index mean and $\mathcal{V}$-index median. In Table 3.5 are represented the thresholds values that have been selected for each of the variables. Threshold values for $\mathcal{V}$-index mean, $\mathcal{V}$-index median and $\mathcal{V}$-index value on the FS are similar to thresholds found in [20], where a $\mathcal{V}$-index greater than 36 ms appears to be associated with dead patients. The creatinine selected threshold value of 1.2 mg/dL is in accordance with [41], where they stated that for the adult male a normal range is from 0.6 to 1.2 mg/dL, while for the adult female a normal range between 0.5 and 1.1 mg/dL.
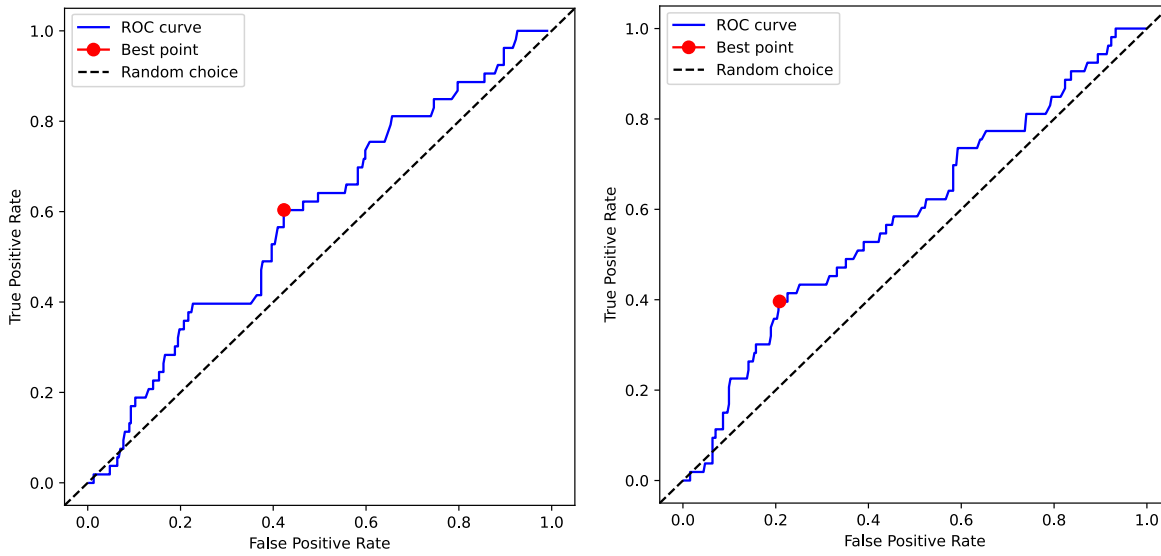
Figure 3.14: The ROC curve for the $\mathcal{V}$-index mean (on the left) and $\mathcal{V}$-index median (on the right). The red dot represents the best FPR-TPR combination. The dashed line represents the random classifier.

Variable	Threshold
$\mathcal{V}$-index mean, visit 2	33.24 ms
$\mathcal{V}$-index median, visit 2	40.35 ms
$\mathcal{V}$-index standard deviation, visit 2	11.54 ms
$\mathcal{V}$-index mesor, visit 2	26.6 ms
$\mathcal{V}$-index amplitude, visit 2	6.64 ms
$\mathcal{V}$-index signature, visit 2	15.25 ms
$\mathcal{V}$-index on first segment, visit 2	32.81 ms
Creatinine	1.2 mg/dL

Table 3.5: The selected thresholds for each variable that has been binarized.

3.4. Survival analysis

After binarizing the variables, a first step has been made by using the Kaplan-Meier method [42], to assess if the variable alone can separate the starting population into two groups with different survival probabilities.

Three factors are used to describe each subject while conducting the Kaplan-Meier survival analysis:

- Their serial time

- Their status (event occurrence or censored) at the conclusion of their serial period

- The group they are in

The serial times for individual participants are organized from the shortest to the longest, regardless of when they entered the research, to develop survival time probabilities and curves. Using this technique, every subject in the group starts the analysis at the same point and continues to survive until one of them experiences an event. One of two things may occur: either the subject would experience the relevant event or, if the event does not have occurred at the end of the follow-up period, they would be considered as *censored*. In this case, there is no information on whether such a patient would experience the event of interest.

While the Y-axis displays the total likelihood of surviving over a certain period of time, the survival duration for each interval is shown as the lengths of the horizontal lines along the X-axis of serial periods. The interval is terminated when the event of interest occurs. The significance of the vertical lines between the horizontals is that they show how the cumulative probability changes as the curve move forward [43]. The K-M curves of $\mathcal{V}$-index mean and $\mathcal{V}$-index median are plotted in Fig. 3.15, the ones of $\mathcal{V}$-index computed on the first segment and of $\mathcal{V}$-index standard deviation are represented in Fig. 3.17. $\mathcal{V}$-index amplitude and $\mathcal{V}$-index mesor curves are illustrated in Fig. 3.16, while the $\mathcal{V}$-index signature in Fig. 3.18. In each plot the p-value is reported, computed through the nonparametric log-rank test, considering the CV death as endpoint event. For example, considering the $\mathcal{V}$-index mean in visit 2, the survival curves for the group of patients with $\mathcal{V}$-index mean ≥ 33.24 ms and for patients < 33.24 ms are statistically different ($p = 0.019$).
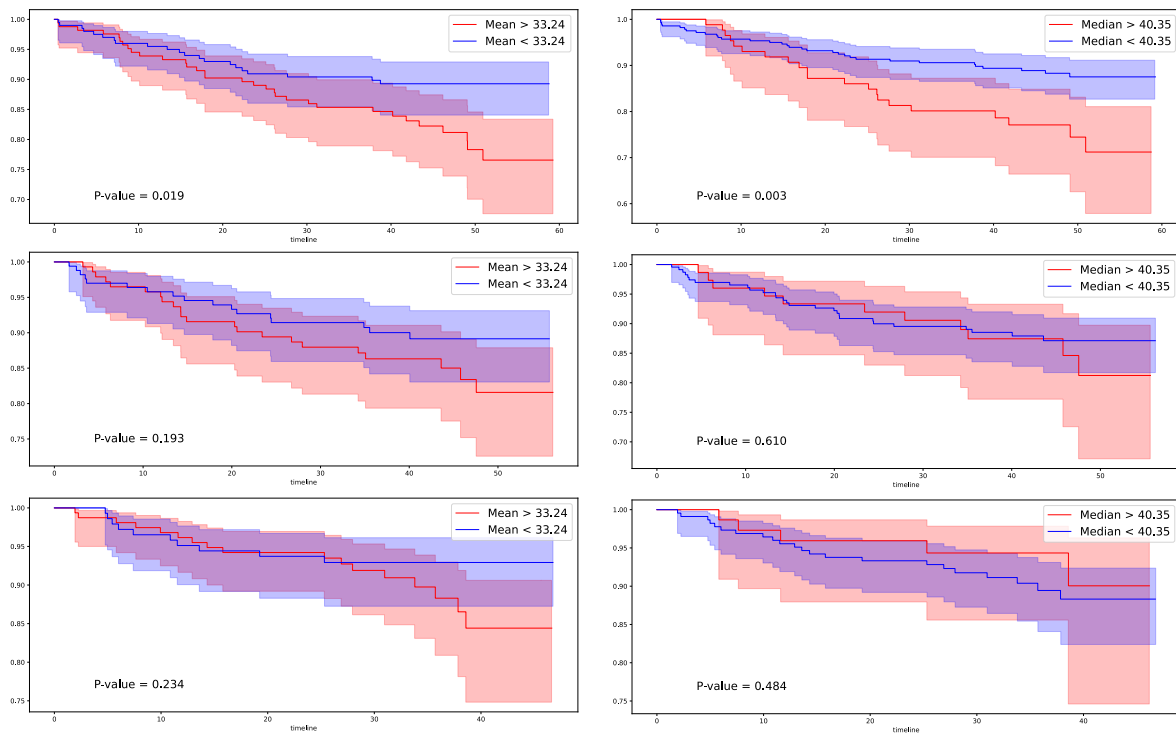
Figure 3.15: Kaplan-Meier curves for $\mathcal{V}$-index meas (on the left) and for $\mathcal{V}$-index median (on the right) are shown for each visit.
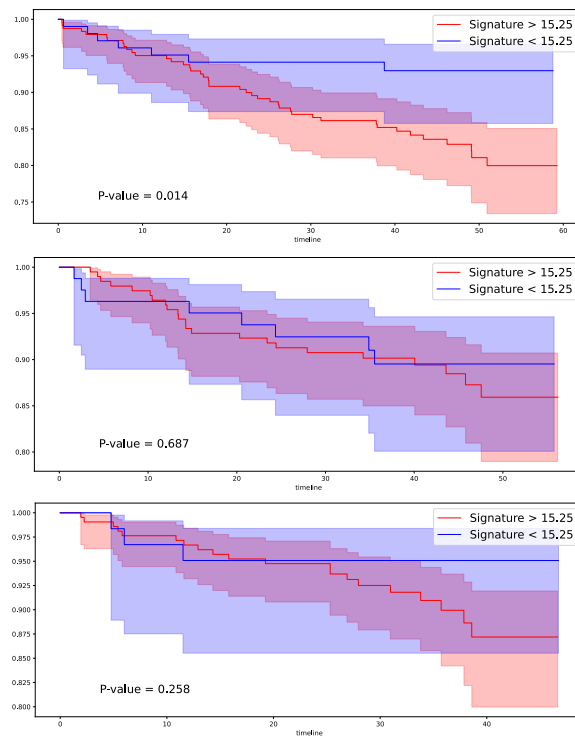

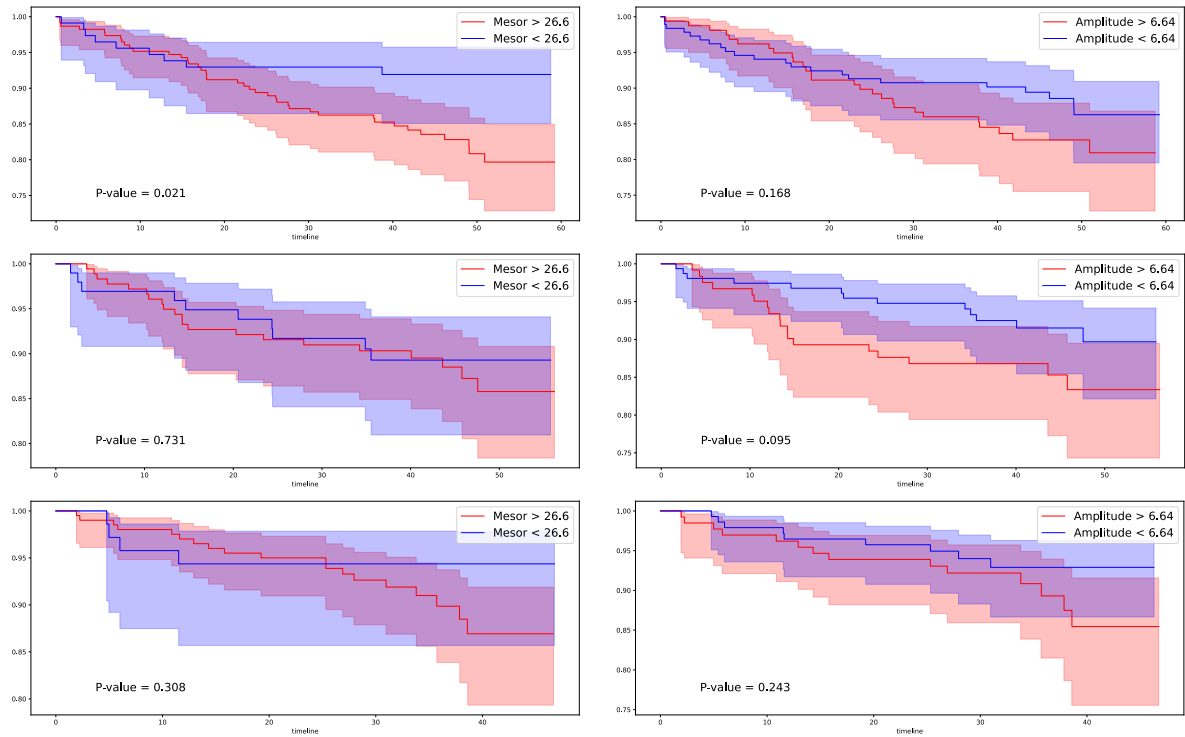Figure 3.18: Kaplan-Meier curves for the $\mathcal{V}$-index signature are shown for each visit.

Figure 3.16: Kaplan-Meier curves for $\mathcal{V}$-index mesor (on the left) and for $\mathcal{V}$-index amplitude (on the right) are shown for each visit.

3.4.1. Visit 2

To evaluate the prognostic capabilities of the $\mathcal{V}$-index, in addition to the K-M method, a first univariate Cox model was used. Then, the $\mathcal{V}$-index was adjusted for age. In the end, $\mathcal{V}$-index was combined with a clinical model, similar to [15], to assess whether its prognostic information was supplementary to conventional prognostic criteria.

Values of the hazard ratio (HR), along with the p-value and concordance index (C-index, also called Harrell's C) of the univariate Cox model computed at the time of visit 2, are represented in Table 3.6. While the HR is the probability of an event in a treatment group relative to the control group probability over a unit of time, the C-index may be seen as the likelihood that, over the course of the same follow-up period, a subject from the event group would have a higher risk score than a subject from the non-event group. Considering a pair of patients (i, j), higher risk should result in a shorter survival time (ST) to the adverse event. So, when the model predicts a higher risk score for patients i, $ST_i < ST_j$ is expected. Defining all the pairs of patients i,j which respects the previous rule as concordant pair, as opposite to discordant pair, the C-index is defined as follows:
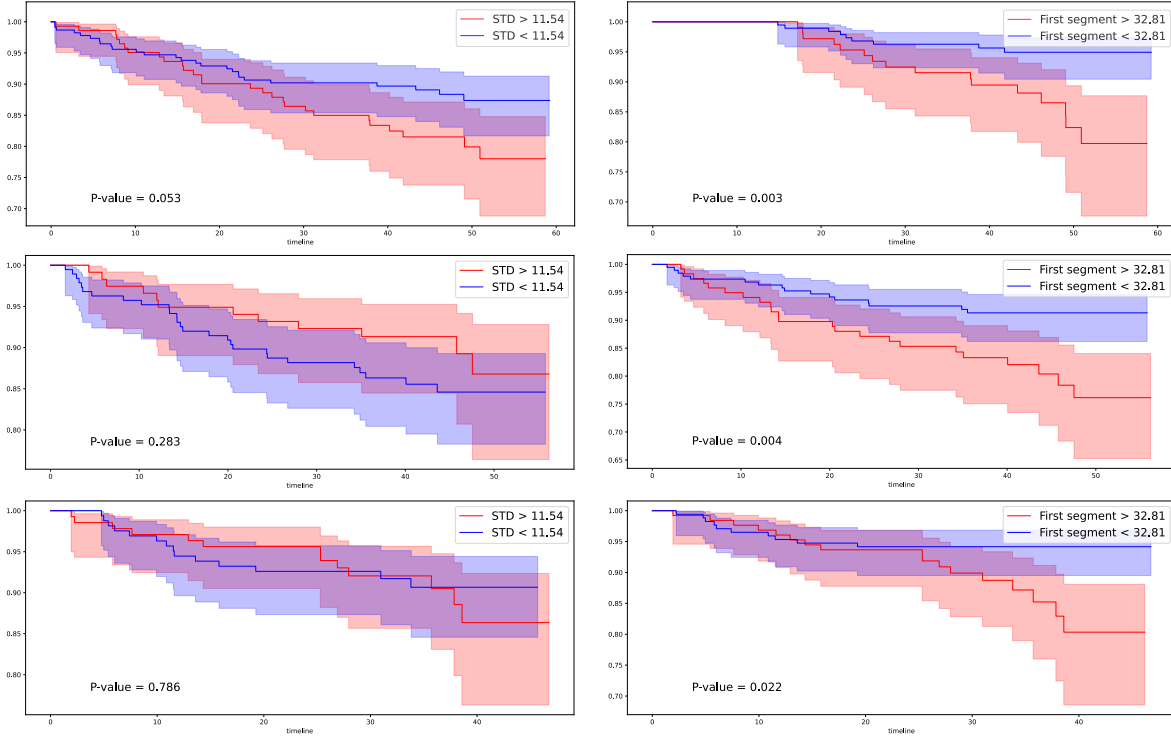
Figure 3.17: Kaplan-Meier curves for $\mathcal{V}$-index standard deviation (on the left) and for the $\mathcal{V}$-index computed on the first segment (on the right) are shown for each visit.

$$C_{index} = \frac{Number\ of\ concordant\ pair}{Number\ of\ comparable\ pair}$$

The pair is excluded, and so considered non-comparable, if neither patient has encountered an event. Also, when just one patient is censored, a pair is only taken into account if the second patient observed the event before the censoring period. Otherwise, it would be impossible to determine which patient may have initially encountered the event, thus the pair is rejected.

At first, a univariate Cox model has been computed for the age, binarized as age ≥ 70 and age<70 years, obtaining an HR=3.66 (95% CI 2.11-6.34), $p < 0.005$ and a C-index of 0.65, considering visit 2. It can be seen in Table 3.6 that greater values of $\mathcal{V}$-index median, mesor, signature and $\mathcal{V}$-index on the FS, all binarized as previously described, are associated with statistical significance ($p < 0.05$) with a higher risk of death. For example, patients with a $\mathcal{V}$-index median value greater than 40.35 ms have double risk of death with respect to patients with $\mathcal{V}$-index median value less than 40.35 ms, in the same follow-up period. The results obtained by adjusting the $\mathcal{V}$-index for age are illustrated in Table 3.7. Overall, considering the variables with $p < 0.05$, joining the $\mathcal{V}$-index brings to

an improvement of the C-index, ranging from the lowest improvement of 4% obtained by using the $\mathcal{V}$-index mean, to the highest improvement of 6% by considering the $\mathcal{V}$-index signature.

	HR (95% CI)	p-value	C-index
$\mathcal{V}$-index mean	1.91 (1.10-3.32)	0.02	0.57
$\mathcal{V}$-index median	2.23 (1.28-3.87)	<0.005	0.58
$\mathcal{V}$-index mesor	2.29 (1.11-4.72)	0.02	0.57
$\mathcal{V}$-index amplitude	1.48 (0.84-2.60)	0.17	0.55
$\mathcal{V}$-index signature	2.64 (1.18-5.87)	0.02	0.58
$\mathcal{V}$-index std	1.69 (0.99-2.90)	0.06	0.56
$\mathcal{V}$-index FS	2.40 (1.39-4.15)	<0.005	0.59

Table 3.6: Results of the univariate Cox models, applied at the time of visit 2.

	HR (95% CI)	p-value	C-index
$\mathcal{V}$-index mean	1.76 (1.02-3.06)	0.04	0.68
$\mathcal{V}$-index median	2.03 (1.17-3.53)	0.01	0.68
$\mathcal{V}$-index mesor	2.05 (0.99-4.23)	0.05	0.69
$\mathcal{V}$-index amplitude	1.43 (0.82-2.52)	0.21	0.69
$\mathcal{V}$-index signature	2.40 (1.08-5.34)	0.03	0.69
$\mathcal{V}$-index std	1.59 (0.93-2.72)	0.09	0.67
$\mathcal{V}$-index FS	2.26 (1.31-3.91)	<0.005	0.69

Table 3.7: Each row represents a multivariate Cox model, composed of the written statistic adjusted for age, applied on the dataset at time visit 2.

When selecting the best multivariate Cox model, for comparison reasons, the same clinical variables in [15] were considered as candidate predictors: age $\geq$ 70 years, sex, ischaemic cardiomyopathy, NYHA class III–IV, LVEF, heart rate, systolic arterial pressure, presence of NSVT, the number of premature ventricular contractions/h, creatinine, sodium, and

presence of beta-blocker (BBL) treatment. In order to prevent overfitting the maximum number of candidate clinical predictors, to combine with one of the $\mathcal{V}$-index metrics, was chosen equal to 4, such that the rule of having maximum z/10 variables is respected, being z the numbers of events (55 CV death events in this case).

The best model selection computed at the time of visit 2 and according to the C-index is composed of age $\geq$ 70 years, creatinine $\geq$ 1.2 mg/dL, presence of NSVT, LVEF and signature $\geq$ 15.25 ms, in detail reported in Table 3.8, obtaining a C-index of 0.78. This represents an improvement with respect to a C-index of 0.76 obtained by the best-performing clinical model, composed of age, creatinine, NSVT and LVEF. Additional results of the best models are shown in Appendix A.4.1.

	HR (95% CI)	p-value
Age $\geq$ 70 years	3.06 (1.69-5.54)	<0.005
Creatinine $\geq$ 1.2 mg/dL	2.78 (1.54-5.02)	<0.005
NSVT	2.12 (1.18-3.82)	<0.005
LVEF	0.96 (0.93-0.99)	0.02
$\mathcal{V}$-signature $\geq$ 15.25 ms	2.56 (1.14-5.72)	0.02

Table 3.8: Results of the best multivariate Cox models, applied at the time of visit 2.

3.4.2.   Visit 4 and visit 6

The same experiments were repeated in visit 4 and visit 6, using the same threshold values found in visit 2. In Appendix (A.2 and A.3) can be found additional results of the models computed using the optimal threshold values (shown in A.1) found for each visit.

The patients (5) who died between visit 2 and 4 were removed, and the starting point of the follow-up was moved at the time of visit 4, so obtaining 375 observations and 50 cardiovascular death events. Then, patients who did not undergo the ECG recording in visit 4 and the ones for which it was not possible to compute $\mathcal{V}$-index in at least one segment were removed, so the number of observations at the time of visit 4 decreased to 292, with 39 CV death events.

The univariate Cox models computed using the $\mathcal{V}$-index obtained in visit 4 are shown in Table 3.9, while in Table 3.10 are presented the multivariate Cox models of the statistics

adjusted for age. The $\mathcal{V}$-index computed on the FS preserves its significance ($p = 0.01$) and values higher than 32.81 ms are associated with higher risk of death.

	HR (95% CI)	p-value	C-index
$\mathcal{V}$-index mean	1.52 (0.81-2.86)	0.20	0.54
$\mathcal{V}$-index median	1.20 (0.60-2.41)	0.61	0.51
$\mathcal{V}$-index std	0.29 (0.35-1.36)	0.29	0.55
$\mathcal{V}$-index mesor	1.02 (0.51-2.04)	0.96	0.49
$\mathcal{V}$-index amplitude	1.89 (0.96-3.72)	0.06	0.59
$\mathcal{V}$-index signature	1.03 (0.49-2.14)	0.94	0.50
$\mathcal{V}$-index FS	2.46 (1.30-4.65)	0.01	0.60

Table 3.9: Results of the univariate Cox models, applied at the time of visit 4.

	HR (95% CI)	p-value	C-index
$\mathcal{V}$-index mean	1.49 (0.79-2.80)	0.22	0.68
$\mathcal{V}$-index median	1.24 (0.62-2.50)	0.54	0.66
$\mathcal{V}$-index std	0.76 (0.38-1.50)	0.43	0.69
$\mathcal{V}$-index mesor	0.98 (0.49-1.97)	0.95	0.67
$\mathcal{V}$-index amplitude	2.19 (1.11-4.33)	0.02	0.71
$\mathcal{V}$-index signature	0.98 (0.47-2.04)	0.95	0.68
$\mathcal{V}$-index FS	2.26 (1.19-4.28)	0.01	0.70

Table 3.10: Each row represents a multivariate Cox model, composed of the written statistic adjusted for age, applied at time visit 4.

The best model selection (reported in Table 3.11), computed at the time of visit 4 and considering only the $\mathcal{V}$-index statistics computed in the ECG recordings registered at visit 4, is the following: age $\geq$ 70 years, NSVT presence, BBL treatment, LVEF, $\mathcal{V}$-index on the FS $\geq$ 32.81 ms, obtaining a C-index of 0.78. The same result (C-index=0.78), is obtained by using age $\geq$ 70 years, creatinine $\geq$ 1.2 mg/dL, BBL treatment, LVEF and $\mathcal{V}$-index amplitude $\geq$ 6.64 ms (HR=2.00, 95% CI 1.01-3.96, $p = 0.05$).

	HR (95% CI)	p-value
Age $\geq$ 70 years	3.04 (1.54-6.03)	<0.005
NSVT	2.02 (1.04-3.92)	0.04
BBL	0.44 (0.23-0.85)	0.01
LVEF	0.96 (0.92-1.00)	0.06
$\mathcal{V}$-index on the FS $\geq$ 32.81 ms	2.19 (1.15-4.18)	0.02

Table 3.11: Results of the best multivariate Cox models, applied at the time of visit 4.

After removing the other 15 patients who died between visit 4 and visit 6, a dataset composed of 360 observations, of which 36 CV death events, is obtained. Removing patients without at least one value of $\mathcal{V}$-index, the dataset obtained is composed of 301 observations, of which 27 CV death events. The univariate Cox models results are presented in Table 3.12, while results for the multivariate Cox models adjusted for age are illustrated in Table 3.13.

Considering only the $\mathcal{V}$-index statistics computed in visit 6, the best model (presented in Table 3.14) is composed by: age $\geq$ 70 years, creatinine $\geq$ 1.2 mg/dL, BBL treatment, NSVT presence and $\mathcal{V}$-index on the FS $\geq$ 32.81 ms, obtaining a C-index of 0.81.

	HR (95% CI)	p-value	C-index
$\mathcal{V}$-index mean	1.60 (0.73-3.50)	0.24	0.53
$\mathcal{V}$-index median	0.71 (0.27-1.87)	0.49	0.53
$\mathcal{V}$-index std	1.11 (0.52-2.36)	0.79	0.49
$\mathcal{V}$-index mesor	1.76 (0.60-5.16)	0.30	0.53
$\mathcal{V}$-index amplitude	1.41 (0.63-3.17)	0.41	0.53
$\mathcal{V}$-index signature	2.00 (0.60-6.70)	0.26	0.54
$\mathcal{V}$-index FS	2.42 (1.11-5.30)	0.03	0.58

Table 3.12: Results of the univariate Cox models, applied at the time of visit 6.

	HR (95% CI)	p-value	C-index
$\mathcal{V}$-index mean	1.56 (0.71-3.41)	0.26	0.70
$\mathcal{V}$-index median	0.68 (0.26-1.80)	0.44	0.70
$\mathcal{V}$-index std	1.15 (0.54-2.45)	0.72	0.68
$\mathcal{V}$-index mesor	1.81 (0.62-5.31)	0.28	0.71
$\mathcal{V}$-index amplitude	1.33 (0.59-2.99)	0.49	0.68
$\mathcal{V}$-index signature	1.94 (0.58-6.50)	0.28	0.71
$\mathcal{V}$-index FS	2.13 (0.97-4.67)	0.06	0.72

Table 3.13: Each row represents a multivariate Cox model, composed of the written statistic adjusted for age, applied on the dataset at time visit 6.

	HR (95% CI)	p-value
Age $\geq$ 70 years	3.04 (1.30-7.12)	0.01
Creatinine $\geq$ 1.2 mg/dL	3.15 (1.36-7.28)	0.01
NSVT	1.94 (0.87-4.33)	0.10
BBL	0.54 (0.25-1.18)	0.12
$\mathcal{V}$-index on the FS $\geq$ 31.82 ms	1.86 (0.84-4.12)	0.13

Table 3.14: Results of the best multivariate Cox models, applied at the time of visit 6.

4 | Discussion

This study shows the potential of using the $\mathcal{V}$-index as a predictor of cardiovascular mortality in heart failure patients. The use of $\mathcal{V}$-index statistics combined with clinical variables increases performances in risk stratification in HF patients. The clinical variables which were found to obtain the best discrimination capabilities are age, serum creatinine, the incidence of NSVT, LVEF, NYHA class and BBL treatment, as confirmed in previous studies which investigated the best set of clinical variables to discriminate among patients at higher risk of death in HF patients [4, 13–15]. Greater values of $\mathcal{V}$-index are associated with a higher risk of death in HF patients, as confirmed in previous study [20, 21] for different conditioned patients.

Considering the $\mathcal{V}$-index statistics analyzed in this study, the median value of the 24h ECG recording appears to be a more robust and reliable parameter with respect to the mean to summarize the $\mathcal{V}$-index behaviour in a day. The application of the cosinor analysis to derive mesor and amplitude provides additional and important information about the daily behaviour of the $\mathcal{V}$-index. The new signature, computed starting from mesor and amplitude, is able to summarize the $\mathcal{V}$-index daily behaviour in a single parameter and gets good performance in discriminating patients that are at higher risk of death. Also considering the $\mathcal{V}$-index computed only on the first segment, the $\mathcal{V}$-index preserves its significance and its prognostic value.

Threshold values found in visit 2 identify at higher risk patients with $\mathcal{V}$-index mean and median value greater than 33.24 ms and 40.35 ms, respectively. Also, values of the $\mathcal{V}$-index signature greater than 15.25 ms are associated with a higher risk of CV death, such as values of the $\mathcal{V}$-index on the first segment greater than 32.81 ms. However, the use of the same thresholds found in visit 2 applied in visit 4 and visit 6 appears to be non-optimal. This can be due to the smaller populations present at the time of visit 4 and visit 6. Indeed, while available observations of $\mathcal{V}$-index in visit 2 were 365, this number has decreased to 307 (-16%) in visit 4 and to 301 in visit 6 (-18%).

In [15] La Rovere et al. investigated the predictive capabilities of Cox models obtained by combining clinical variables (age, creatinine, LVEF and NSVT) and autonomic markers

of the ECG on the (slightly) same population. In particular, they computed the following autonomic markers: SDNN, VLFP, LFP, DFA, TS. Comparing the $\mathcal{V}$-index with these autonomic markers, considering the C-index as the metric to evaluate performances of the Cox model, the results obtained in this study exploit the relevance of $\mathcal{V}$-index in predicting cardiovascular mortality. The best results obtained in this study in visit 2, resulting from multivariate Cox models achieved by combining a clinical model with, respectively, the $\mathcal{V}$-index signature (C-index=0.78), the $\mathcal{V}$-index mesor (C-index=0.78) and $\mathcal{V}$-index median (C-index=0.76), are in line with results obtained in [15] with SDNN (0.76), the logarithm of VLFP (0.79), the logarithm of LFP (0.79), DFA (0.76) and TS (0.75).

In conclusion, this study shows that the use of $\mathcal{V}$-index has a relevant prognostic value in HF patients and its use should be further investigated.

Bibliography

[1] E. E. van Riet, A. W. Hoes, K. P. Wagenaar, A. Limburg, M. A. Landman, and F. H. Rutten, "Epidemiology of heart failure: the prevalence of heart failure and ventricular dysfunction in older adults over time. a systematic review," *European Journal of Heart Failure*, vol. 18, pp. 242–252, jan 2016.

[2] A. Groenewegen, F. H. Rutten, A. Mosterd, and A. W. Hoes, "Epidemiology of heart failure," *European Journal of Heart Failure*, vol. 22, pp. 1342–1356, jun 2020.

[3] S. Dassanayaka and S. P. Jones, "Recent developments in heart failure," *Circulation Research*, vol. 117, sep 2015.

[4] A. Inamdar and A. Inamdar, "Heart failure: Diagnosis, management and utilization," *Journal of Clinical Medicine*, vol. 5, p. 62, jun 2016.

[5] T. Ohtani, S. F. Mohammed, K. Yamamoto, S. M. Dunlay, S. A. Weston, Y. Sakata, R. J. Rodeheffer, V. L. Roger, and M. M. Redfield, "Diastolic stiffness as assessed by diastolic wall strain is associated with adverse remodelling and poor outcomes in heart failure with preserved ejection fraction," *European Heart Journal*, vol. 33, pp. 1742–1749, may 2012.

[6] C. W. Yancy, M. Jessup, B. Bozkurt, J. Butler, D. E. Casey, M. H. Drazner, G. C. Fonarow, S. A. Geraci, T. Horwich, J. L. Januzzi, M. R. Johnson, E. K. Kasper, W. C. Levy, F. A. Masoudi, P. E. McBride, J. J. McMurray, J. E. Mitchell, P. N. Peterson, B. Riegel, F. Sam, L. W. Stevenson, W. W. Tang, E. J. Tsai, and B. L. Wilkoff, "2013 ACCF/AHA guideline for the management of heart failure," *Journal of the American College of Cardiology*, vol. 62, pp. e147–e239, oct 2013.

[7] R. D. S. Watson, "ABC of heart failure: Clinical features and complications," *BMJ*, vol. 320, pp. 236–239, jan 2000.

[8] S. J. Pocock, D. Wang, M. A. Pfeffer, S. Yusuf, J. J. McMurray, K. B. Swedberg, J. Ostergren, E. L. Michelson, K. S. Pieper, and C. B. Granger, "Predictors of mortality and morbidity in patients with chronic heart failure," *European Heart Journal*, vol. 27, pp. 65–75, oct 2005.

[9] G. C. Fonarow, "Adherence to heart failure quality-of-care indicators in US hospitals," *Archives of Internal Medicine*, vol. 165, p. 1469, jul 2005.

[10] J. L. Januzzi, R. Sakhuja, M. O'Donoghue, A. L. Baggish, S. Anwaruddin, C. U. Chae, R. Cameron, D. G. Krauser, R. Tung, C. A. Camargo, and D. M. Lloyd-Jones, "Utility of amino-terminal pro–brain natriuretic peptide testing for prediction of 1-year mortality in patients with dyspnea treated in the emergency department," *Archives of Internal Medicine*, vol. 166, p. 315, feb 2006.

[11] R. West, L. Liang, G. C. Fonarow, R. Kociol, R. M. Mills, C. M. O'Connor, and A. F. Hernandez, "Characterization of heart failure patients with preserved ejection fraction: a comparison between ADHERE-US registry and ADHERE-international registry," *European Journal of Heart Failure*, vol. 13, pp. 945–952, sep 2011.

[12] W. Ouwerkerk, A. A. Voors, and A. H. Zwinderman, "Factors influencing the predictive power of models for predicting mortality and/or heart failure hospitalization in patients with heart failure," *JACC: Heart Failure*, vol. 2, pp. 429–436, oct 2014.

[13] T. Ahmad, A. Munir, S. H. Bhatti, M. Aftab, and M. A. Raza, "Survival analysis of heart failure patients: A case study," *PLOS ONE*, vol. 12, p. e0181001, jul 2017.

[14] S. Barlera, L. Tavazzi, M. G. Franzosi, R. Marchioli, E. Raimondi, S. Masson, R. Urso, D. Lucci, G. L. Nicolosi, A. P. Maggioni, and G. Tognoni, "Predictors of mortality in 6975 patients with chronic heart failure in the gruppo italiano per lo studio della streptochinasi nell'infarto miocardico-heart failure trial," *Circulation: Heart Failure*, vol. 6, pp. 31–39, jan 2013.

[15] M. T. L. Rovere, G. D. Pinna, R. Maestri, S. Barlera, M. Bernardinangeli, M. Veniani, G. L. Nicolosi, R. Marchioli, and L. T. and, "Autonomic markers and cardiovascular and arrhythmic events in heart failure patients: still a place in prognostication? data from the GISSI-HF trial," *European Journal of Heart Failure*, vol. 14, pp. 1410–1419, dec 2012.

[16] R. Sassi and L. T. Mainardi, "An estimate of the dispersion of repolarization times based on a biophysical model of the ECG," *IEEE Transactions on Biomedical Engineering*, vol. 58, pp. 3396–3405, dec 2011.

[17] R. Abächerli, R. Twerenbold, J. Boeddinghaus, T. Nestelberger, P. Mächler, R. Sassi, M. W. Rivolta, E. K. Roonizi, L. T. Mainardi, N. Kozhuharov, M. R. Giménez, K. Wildi, K. Grimm, Z. Sabti, P. Hillinger, C. Puelacher, I. Strebel, J. Cupa, P. Badertscher, I. Roux, R. Schmid, R. Leber, S. Osswald, C. Mueller, and T. Reichlin, "Diagnostic and prognostic values of the v-index, a novel ECG marker quantifying

spatial heterogeneity of ventricular repolarization, in patients with symptoms suggestive of non-ST-elevation myocardial infarction," *International Journal of Cardiology*, vol. 236, pp. 23–29, jun 2017.

[18] M. W. Rivolta, L. T. Mainardi, and R. Sassi, "Quantification of ventricular repolarization heterogeneity during moxifloxacin or sotalol administration using v-index," *Physiological Measurement*, vol. 36, pp. 803–811, mar 2015.

[19] V. Corino, R. Sassi, L. Mainardi, and M. Rivolta, "Assessment of spatial heterogeneity of ventricular repolarization after quinidine in healthy subjects," in *Computing in Cardiology Conference (CinC)*, Computing in Cardiology, sep 2017.

[20] M. W. Rivolta, L. T. Mainardi, R. C. Reis, M. O. C. Rocha, A. L. P. Ribeiro, F. Lombardi, and R. Sassi, "Spatial repolarization heterogeneity and survival in chagas disease," *Methods of Information in Medicine*, vol. 53, no. 06, pp. 464–468, 2014.

[21] M. W. Rivolta, L. T. Mainardi, R. Laureanti, R. Sassi, M. Kühne, N. Rodondi, G. Conte, G. Moschovitis, V. Schlageter, S. Aeschbacher, D. Conen, T. Reichlin, L. Roten, S. Osswald, C. S. Zuern, A. Auricchio, and V. D. Corino, "Association between ventricular repolarization parameters and cardiovascular death in patients of the SWISS-AF cohort," *International Journal of Cardiology*, vol. 356, pp. 53–59, jun 2022.

[22] G.-H. investigators, "Effect of rosuvastatin in patients with chronic heart failure (the GISSI-HF trial): a randomised, double-blind, placebo-controlled trial," *The Lancet*, vol. 372, pp. 1231–1239, oct 2008.

[23] M. Canepa, P. L. Temporelli, A. Rossi, A. Rossi, L. Gonzini, G. L. Nicolosi, L. Staszewsky, R. Marchioli, A. P. Maggioni, and L. T. and, "Prevalence and prognostic impact of chronic obstructive pulmonary disease in patients with chronic heart failure: Data from the GISSI-HF trial," *Cardiology*, vol. 136, pp. 128–137, sep 2016.

[24] S. Sendelbach and M. Funk, "Alarm fatigue," *AACN Advanced Critical Care*, vol. 24, pp. 378–386, oct 2013.

[25] G. Friesen, T. Jannett, M. Jadallah, S. Yates, S. Quint, and H. Nagle, "A comparison of the noise sensitivity of nine QRS detection algorithms," *IEEE Transactions on Biomedical Engineering*, vol. 37, no. 1, pp. 85–98, 1990.

[26] P. C. Bhaskar, "Reduction of power line interference in ecg signal using fir filter," 2012.

[27] U. Satija, B. Ramkumar, and M. S. Manikandan, "A review of signal processing tech-

niques for electrocardiogram signal quality assessment," *IEEE Reviews in Biomedical Engineering*, vol. 11, pp. 36–52, 2018.

[28] Y. Luo, R. H. Hargraves, A. Belle, O. Bai, X. Qi, K. R. Ward, M. P. Pfaffenberger, and K. Najarian, "A hierarchical method for removal of baseline drift from biomedical signals: Application in ECG analysis," *The Scientific World Journal*, vol. 2013, pp. 1–10, 2013.

[29] F. Azuaje, G. Clifford, and P. McSharry, *Advanced Methods and Tools for ECG Data Analysis*, vol. 6. Springer Nature, 2006.

[30] Q. Li, R. G. Mark, and G. D. Clifford, "Artificial arterial blood pressure artifact models and an evaluation of a robust blood pressure and heart rate estimator," *BioMedical Engineering OnLine*, vol. 8, jul 2009.

[31] I. Silva, J. Lee, and R. G. Mark, "Signal quality estimation with multichannel adaptive filtering in intensive care settings," *IEEE Transactions on Biomedical Engineering*, vol. 59, pp. 2476–2485, sep 2012.

[32] U. Satija, B. Ramkumar, and M. S. Manikandan, "Automated ECG noise detection and classification system for unsupervised healthcare monitoring," *IEEE Journal of Biomedical and Health Informatics*, vol. 22, pp. 722–732, may 2018.

[33] M. E. Torres, M. A. Colominas, G. Schlotthauer, and P. Flandrin, "A complete ensemble empirical mode decomposition with adaptive noise," in *2011 IEEE International Conference on Acoustics, Speech and Signal Processing (ICASSP)*, IEEE, May 2011.

[34] R. M. Rangayyan, *Biomedical Signal Analysis*. IEEE Press Series on Biomedical Engineering, Hoboken, NJ: Wiley-Blackwell, 2 ed., May 2015.

[35] A. van Oosterom, "ECGSIM: an interactive tool for studying the genesis of QRST waveforms," *Br. Heart J.*, vol. 90, pp. 165–168, Feb. 2004.

[36] R. Sassi, L. T. Mainardi, P. Laguna, and J. F. Rodriguez, "Validation of the -index through finite element 2d simulations," in *Computing in Cardiology 2013*, vol. 40, pp. 337–340, 2013.

[37] D. R. Cox, "Regression models and life-tables," *Journal of the Royal Statistical Society: Series B (Methodological)*, vol. 34, no. 2, pp. 187–202, 1972.

[38] T. Therneau and P. Grambsch, *Modeling survival data: Extending the cox model*. Statistics for Biology and Health, New York, NY: Springer, 1 ed., Dec. 2000.

[39] G. Cornelissen, "Cosinor-based rhythmometry," *Theoretical Biology and Medical Modelling*, vol. 11, apr 2014.

[40] K. Hajian-Tilaki, "Receiver operating characteristic (ROC) curve analysis for medical diagnostic test evaluation," *Caspian J. Intern. Med.*, vol. 4, no. 2, pp. 627–635, 2013.

[41] H. K. Walker, W. D. Hall, and J. W. Hurst, *Clinical Methods: The History, Physical, and Laboratory Examinations*. Boston: Butterworths, 1990.

[42] E. L. Kaplan and P. Meier, "Nonparametric estimation from incomplete observations," *Journal of the American Statistical Association*, vol. 53, pp. 457–481, jun 1958.

[43] J. T. Rich, J. G. Neely, R. C. Paniello, C. C. J. Voelker, B. Nussenbaum, and E. W. Wang, "A practical guide to understanding kaplan-meier curves," *Otolaryngology–Head and Neck Surgery*, vol. 143, pp. 331–336, sep 2010.

A | Appendix A

A.1. Thresholds

The optimezed threshold values that have been found for $\mathcal{V}$-index statistics in visit 4 and visit 6 are represented in Table A.1.

	Threshold
$\mathcal{V}$-index means, visit 4	39.36 ms
$\mathcal{V}$-index means, visit 6	35.11 ms
$\mathcal{V}$-index medians, visit 4	36.43 ms
$\mathcal{V}$-index medians, visit 6	33.31 ms
$\mathcal{V}$-index std, visit 4	9.3 ms
$\mathcal{V}$-index std, visit 6	14.3 ms
$\mathcal{V}$-index mesor, visit 4	39.50 ms
$\mathcal{V}$-index mesor, visit 6	34.45 ms
$\mathcal{V}$-index amplitude, visit 4	7.30 ms
$\mathcal{V}$-index amplitude, visit 6	6.80 ms
$\mathcal{V}$-index signature, visit 4	21.62 ms
$\mathcal{V}$-index signature, visit 6	19.95 ms
$\mathcal{V}$-index first segment, visit 4	34.16 ms
$\mathcal{V}$-index first segment, visit 6	33.47 ms

Table A.1: The selected thresholds for each variable that has been binarized.

In the following chapters are presented the models that have been computed in visit 4 and 6 by using the optimized thresholds.

A.2.   Visit 4

In Table A.2 the univariate Cox models computed with the $\mathcal{V}$-index obtained in visit 4 are shown, while in Table A.3 the multivariate Cox models of the statistics are adjusted for age. Also in this case, with different thresholds, the $\mathcal{V}$-index statistics preserve their significance and higher values are associated with a higher risk of death.

	HR (95% CI)	p-value	C-index
$\mathcal{V}$-index mean	1.88 (1.00-3.55)	0.05	0.56
$\mathcal{V}$-index median	2.15 (1.15-4.03)	0.02	0.58
$\mathcal{V}$-index mesor	2.06 (1.06-4.03)	0.03	0.58
$\mathcal{V}$-index amplitude	2.00 (1.02-3.91)	0.04	0.59
$\mathcal{V}$-index signature	2.02 (1.04-3.93)	0.04	0.58
$\mathcal{V}$-index std	1.45 (0.76-2.76)	0.26	0.54
$\mathcal{V}$-index FS	2.78 (1.47-5.26)	<0.005	0.61

Table A.2: Results of the univariate Cox models, applied at the time of visit 4.

	HR (95% CI)	p-value	C-index
$\mathcal{V}$-index mean	1.97 (1.05-3.71)	0.04	0.69
$\mathcal{V}$-index median	2.14 (1.14-4.01)	0.02	0.69
$\mathcal{V}$-index mesor	2.09 (1.07-4.08)	0.03	0.69
$\mathcal{V}$-index amplitude	2.34 (1.19-4.59)	0.01	0.71
$\mathcal{V}$-index signature	2.06 (1.06-3.99)	0.03	0.70
$\mathcal{V}$-index std	0.44 (0.81-2.97)	0.18	0.68
$\mathcal{V}$-index FS	2.62 (1.38-4.96)	<0.005	0.71

Table A.3: Each row represents a multivariate Cox model, composed of the written statistic adjusted for age, applied at time visit 4.

The best model selection (reported in Table A.4), computed at the time of visit 4 and considering only the $\mathcal{V}$-index statistics computed in the ECG recordings registered at visit

4, is the following: age $\geq$ 70 years, NSVT presence, BBL treatment, LVEF, $\mathcal{V}$-index on the FS $\geq$ 34.16 ms, obtaining a C-index of 0.787. A similar result (C-index=0.776), is obtained by using age $\geq$ 70 years, creatinine $\geq$ 1.2 mg/dL, BBL treatment, LVEF and amplitude $\geq$ 7.30 ms (HR=2.04, 95% CI 1.03-4.02, $p = 0.04$). Additional results can be found in Section A.4.2.

	HR (95% CI)	p-value
Age $\geq$ 70 years	3.07 (1.55-6.07)	<0.005
NSVT	1.99 (1.02-3.87)	0.04
BBL	0.45 (0.23-0.86)	0.02
LVEF	0.96 (0.92-1.00)	0.06
$\mathcal{V}$-index on the FS $\geq$ 34.16 ms	2.54 (1.34-4.83)	<0.005

Table A.4: Results of the best multivariate Cox models, applied at the time of visit 4.

A.3. Visit 6

The univariate Cox models have been computed as previously described, and results are presented in Table A.5. Results for the multivariate Cox models adjusted for age are illustrated in Table A.6.

Considering only the $\mathcal{V}$-index variables computed in visit 6, the best model (Table A.7) is composed by: age $\geq$ 70 years, creatinine $\geq$ 1.2 mg/dL, LVEF, NSVT presence and $\mathcal{V}$-index cosinor (computed in visit 6) $\geq$ 19.95 ms, obtaining a C-index of 0.82. Additional results can be found in Section A.4.2.

	HR (95% CI)	p-value	C-index
$\mathcal{V}$-index mean	2.11 (0.96-4.61)	0.06	0.56
$\mathcal{V}$-index median	2.28 (1.04-4.98)	0.04	0.57
$\mathcal{V}$-index mesor	2.21 (0.96-5.05)	0.06	0.57
$\mathcal{V}$-index amplitude	1.44 (0.64-3.24)	0.38	0.53
$\mathcal{V}$-index signature	2.63 (1.09-6.34)	0.03	0.59
$\mathcal{V}$-index std	1.39 (0.65-3.00)	0.40	0.51
$\mathcal{V}$-index FS	2.73 (1.25-5.97)	0.01	0.59

Table A.5: Results of the univariate Cox models, applied at the time of visit 6.

	HR (95% CI)	p-value	C-index
$\mathcal{V}$-index mean	1.97 (0.90-4.32)	0.09	0.71
$\mathcal{V}$-index median	2.17 (0.99-4.75)	0.05	0.72
$\mathcal{V}$-index mesor	2.21 (0.97-5.06)	0.06	0.72
$\mathcal{V}$-index amplitude	1.34 (0.59-3.02)	0.48	0.68
$\mathcal{V}$-index signature	2.83 (1.17-6.82)	0.02	0.73
$\mathcal{V}$-index std	1.68 (0.78-3.64)	0.19	0.69
$\mathcal{V}$-index FS	2.40 (1.09-5.25)	0.03	0.73

Table A.6: Each row represents a multivariate Cox model, composed of the written statistic adjusted for age, applied on the dataset at time visit 6.

	HR (95% CI)	p-value
Age $\geq$ 70 years	3.59 (1.46-8.80)	0.01
Creatinine $\geq$ 1.2 mg/dL	3.83 (1.48-9.90)	0.01
NSVT	2.07 (0.89-4.80)	0.09
LVEF	0.99 (0.95-1.03)	0.61
$\mathcal{V}$-index signature $\geq$ 19.95 ms	2.13 (0.87-5.21)	0.10

Table A.7: Results of the best multivariate Cox models, applied at the time of visit 6.

A.4.   Best models

A.4.1.   Same thresholds

In the following are represented the best models obtained in visit 2 (Table A.8), visit 4 (Table A.9) and visit 6 (Table A.10), obtained using the thresholds found in visit 2.

Variables	C-index
age, creatinine, NSVT, LVEF, $\mathcal{V}$-index signature	0.78
age, creatinine, NSVT, LVEF, $\mathcal{V}$-index mesor	0.78
age, creatinine, NYHA class, LVEF, Signature	0.78
age, creatinine, NYHA class, LVEF, $\mathcal{V}$-index on the FS	0.77
age, creatinine, NSVT, LVEF, $\mathcal{V}$-index median	0.76

Table A.8: Best models that have been found at time visit 2.

Variables	C-index
age, NSVT, BBL, LVEF, $\mathcal{V}$-index on the first segment (v4)	0.78
age, creatinine, BBL, LVEF, $\mathcal{V}$-index amplitude (v4)	0.78
age, NYHA class, BBL, LVEF, $\mathcal{V}$-index amplitude (v4)	0.78
age, NSVT, BBL, LVEF, $\mathcal{V}$-index amplitude (v4)	0.77
age, creatinine, NYHA class, LVEF, $\mathcal{V}$-index amplitude (v4)	0.77

Table A.9: Best models that have been found at time visit 4.

Variables	C-index
age, creatinine, NSVT, LVEF, $\mathcal{V}$-index signature (v6)	0.82
age, creatinine, NSVT, SEX (M), TVNS, $\mathcal{V}$-index amplitude (v6)	0.82
age, creatinine, NSVT, BBL, $\mathcal{V}$-index median (v6)	0.81
age, creatinine, NSVT, BBL, $\mathcal{V}$-index mean (v6)	0.81
age, creatinine, NSVT, BBL, $\mathcal{V}$-index on FS (v6)	0.80

Table A.10: Best models that have been found at time visit 6.

A.4.2. Optimized thresholds

In the following are represented the best models obtained in visit 4 (Table A.11) and visit 6 (Table A.12), obtained using the optimized threshold found in each visit.

Variables	C-index
age, NSVT, BBL, LVEF, $\mathcal{V}$-index on the first segment (v4)	0.79
age, creatinine, BBL, LVEF, $\mathcal{V}$-index amplitude (v4)	0.78
age, NYHA class, NSVT, LVEF, $\mathcal{V}$-index median (v4)	0.77
age, NYHA class, NSVT, LVEF, signature (v4)	0.77
age, LVEF, BBL, NSVT, $\mathcal{V}$-index median (v4)	0.77

Table A.11: Best models that have been found at time visit 4.

Variables	C-index
age, creatinine, NSVT, LVEF, $\mathcal{V}$-index signature (v6)	0.82
age, creatinine, NSVT, SEX (M), TVNS, $\mathcal{V}$-index amplitude (v6)	0.82
age, creatinine, NSVT, BBL, $\mathcal{V}$-index median (v6)	0.81
age, creatinine, NSVT, BBL, $\mathcal{V}$-index mean (v6)	0.81
age, creatinine, NSVT, BBL, $\mathcal{V}$-index on FS (v6)	0.80

Table A.12: Best models that have been found at time visit 6.

List of Figures

List of Tables

Ringraziamenti

Prima di tutto, desidero porgere un sentito ringraziamento alla mia relatrice, la Prof. Valentina Corino, e ad i miei correlatori, il Prof. Jose Felix Rodriguez Matas ed il Prof Massimo Walter Rivolta, per avermi assegnato un progetto di notevole interesse ed avermi aiutato, con pazienza e dedizione, in questo lungo percorso.

Voglio ringraziare più di tutti mamma e papà, che mi hanno permesso di poter affrontare tutto il percorso di studi in completa serenità, senza dovermi preoccupare di altro se non studiare. Spero che oggi ancor più di ieri siate fieri di me. Voglio ringraziare anche Anna, Diego e soprattuto la piccola Emily, che ha portato tanta felicità in famiglia.

Voglio ringraziare Carme, che per mesi si è sorbita le mie lamentele, preoccupazioni e stati d'angoscia, sempre appoggiandomi e standomi vicino. Grazie di credere in me più di ogni altro.

Infine voglio ringraziare tutti i miei amici, in particolare Checco, Enri, Fabri, Mario, Manfre, Volpe, Pierpaolo, Bacco, Garba, Pasto, Dili, Lodz e Chiara, per essermi sempre stati vicini e aver condiviso con me tutti i momenti di gioia.